Catalytic Behaviour of Anionic Metalloporphyrins towards the Synthesis of Water- Soluble Polyaniline

‘Mathese Palesa Phooko

Supervisor: Ass.Prof. M. Sekota

Department of Chemistry and Chemical Technology

National University of Lesotho

Dissertation submitted in fulfilment of the requirements for the degree of Masters of Science

Abstract

In this study, metalloderivates of anionic tetrasulphonated tetraphenyl porphyrin ($MTPPS_4$, where M= Ru(III) and Rh(III)) were synthesized and characterized and later utilized in the synthesis of water-soluble Polyaniline (PANi). The selected metalloporphyrins were synthesized with very low percentage yields. It was found that the $RUTPPS_4$ was more effective as the homogeneous catalyst than $RhTPPS_4$ as it showed a high turnover. This was attributed to the size of Ru^{3+} and the relative ease of oxidation of Ru(III) to Ru(IV). The synthesis and properties of PANi prepared are reported. The processabilty of the polymer was examined and it was found to be soluble in water and polar aprotic solvents like dimethyl formamide (DMF). The clewed nanostructured porous PANi exhibited rich electrochemical features which are interesting in the field of sensors and actuators.

CHAPTER 1

1.0 INTRODUCTION

1.1 Metalloporphyrins

Porphyrins (Greek for "purple") are a class of macrocyclic compounds and are based on 16 Carbon atom ring containing four nitrogen atoms. The four pyrrole rings are linked via four methine bridges as shown in Figure 1.1a. They are aromatic as they obey Huckel's theory for aromaticity in that they possess $(4n + 2)\pi$ electrons that are delocalized over the macrocycle. The macrocycles, therefore, are highly conjugated systems and this conjugated π-system is the electronic "heart" of the macrocycle and is responsible for the intensity, colour and optical properties of porphyrins. Porphyrins are mostly symmetrical and they likely form organized face-to-face aggregates through π–π stacking. This is called self-assembly. Since porphyrins accept or donate electrons easily through their large π-electron frameworks, they are suitable for electronic conduction, and together with their optical properties, porphyrins have become one of more studied frame structures in organic optoelectronic devices [1].

Related macrocycles include the phthalocyanines in which the isoindole units are linked by imine bridges as shown in Figure 1.1b. Related biologically important macrocycles are chlorophylls (which have a central magnesium ion) and pheophytins (which are metal free) in the photosynthetic apparatus of plants and bacteria and vitamin B-12 (which has cobalt) found in bacteria and animals.

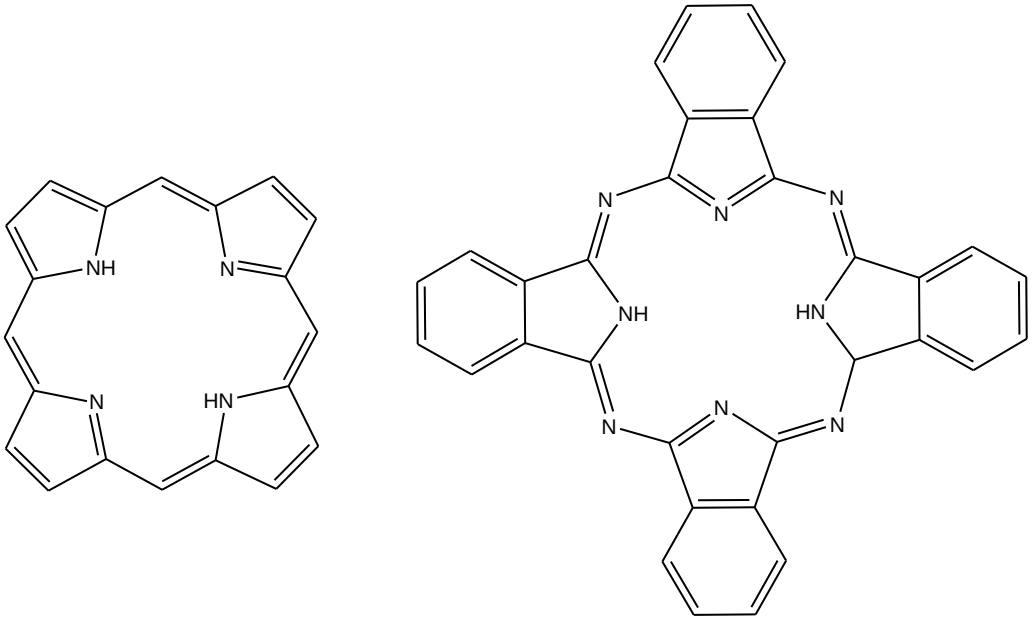

(a) (b)

Figure 1.1: Molecular structures of a) Porphyrin and b) phthalocyanine.

1.1.1 Porphyrin Variation

The porphyrin basic structure could be varied in so many ways, thus there is a large number of porphyrins. Substitution at any of the positions in the inner or outer carbon atoms changes the properties of the macrocycle. The substitutions on the outer carbon atoms could be done on the meso (*) or beta (*) positions as in Figure 1.2.

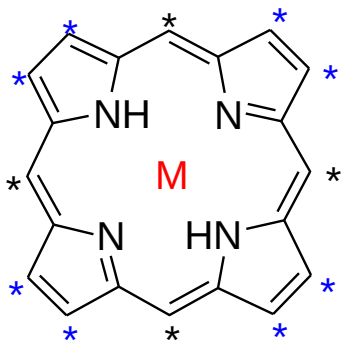

Figure1.2: Meso (*) and beta (*) positions on porphyrin macrocycle.

For instance, the presence of the sulphonatophenyl group on the meso positions of the parent ring renders the porphyrin water soluble. Zinc(II) tetraphenylporphyrin is insoluble in water while its sulphonated derivative tetrasulphonatotetraphenyl porphyrin, is water soluble (Figure 1.3).

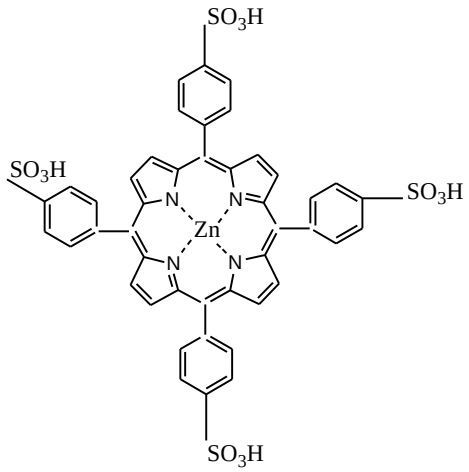

$ZnTPPS_4$

Figure1.3: chemical structure of tetrasulphonatotetraphenyl porphyrin, $ZnTPPS_4$

The porphyrin nucleus is a tetradentate ligand in which the space available for a coordinated metal has a maximum diameter of approximately 3.7Å, thus they are of perfect size to bind nearly all metal ions to form the metalloporphyrins [2]. Thus the metalloporphyrins are complexes of porphyrins. Unlike other macrocyclic ligands, for example crown ethers, porphyrins are not selective as the cavity is quite accommodative. Metalloporphyrins are one of the cornerstones on which the existence of life is based and major biochemical, enzymatic, and photochemical functions depend on the special properties of a tetrapyrrolic macrocycle [3]. Due to their primary participation in the photosynthesis process and their unique electronic, magnetic and optical properties, many studies on the development of electronic and energy conversion devices incorporate porphyrins, and several related metallized and unmetallized tetrapyrrolic compounds [2].

1.1.2 Synthesis of Metalloporphyrins

Almost all metals form 1:1 complexes with porphyrins although Na, K and Li complexes are 2:1 in which the metal atoms are incorporated slightly below and above the porphyrin macrocycle plane [4]. The ability of metalloporphyrins to form intermolecular bonds based on axial coordination of ligands with central metals is inherent in many square-planar complexes, ML_4 [5]. The hardness or softness and the coordination number of the metal ion determine the extent of extra coordination with various ligands. For instance, Metals such as Ru and Os can form very strong complexes with axially coordinated ligands, and the corresponding supramolecular structures are stable in wide variety of conditions.

The porphyrin complexes with transition metal ions are very stable, for instance, the stability constant for Zinc (II) tetraphenylporphyrin is 10^{29} [2]. It must be noted that when coordination occurs, two protons are removed from the pyrrole nitrogen atoms, leaving two negative charges on the ring as per scheme 1;

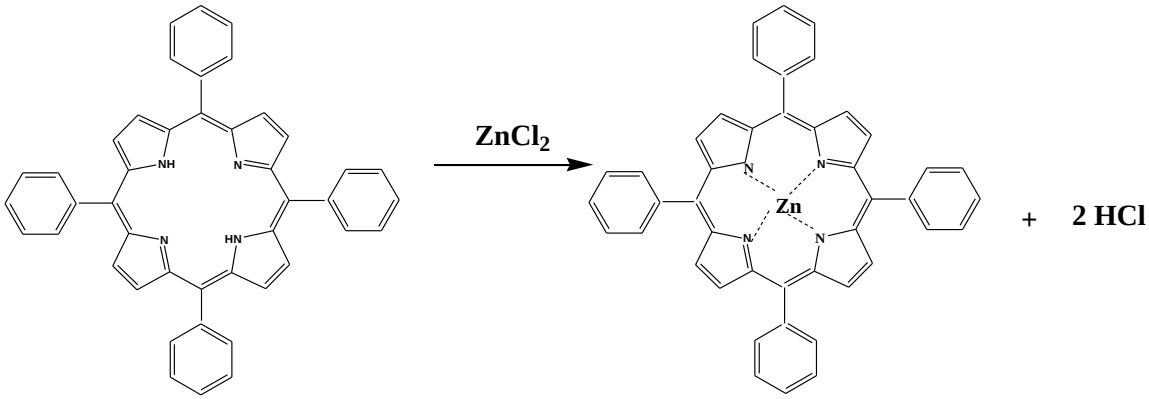

TPP

Scheme 1: Deprotonation of porphyrin during coordination

Metalloporphyrins can be prepared by various methods but the classic synthetic route is reaction of any aromatic aldehyde and pyrrole in acidic medium for example propionic acid. The corresponding salt is added to the porphyrin in weakly coordinating solvents like dimethyl formamide (DMF). The reaction is carried out with heating and refluxing.

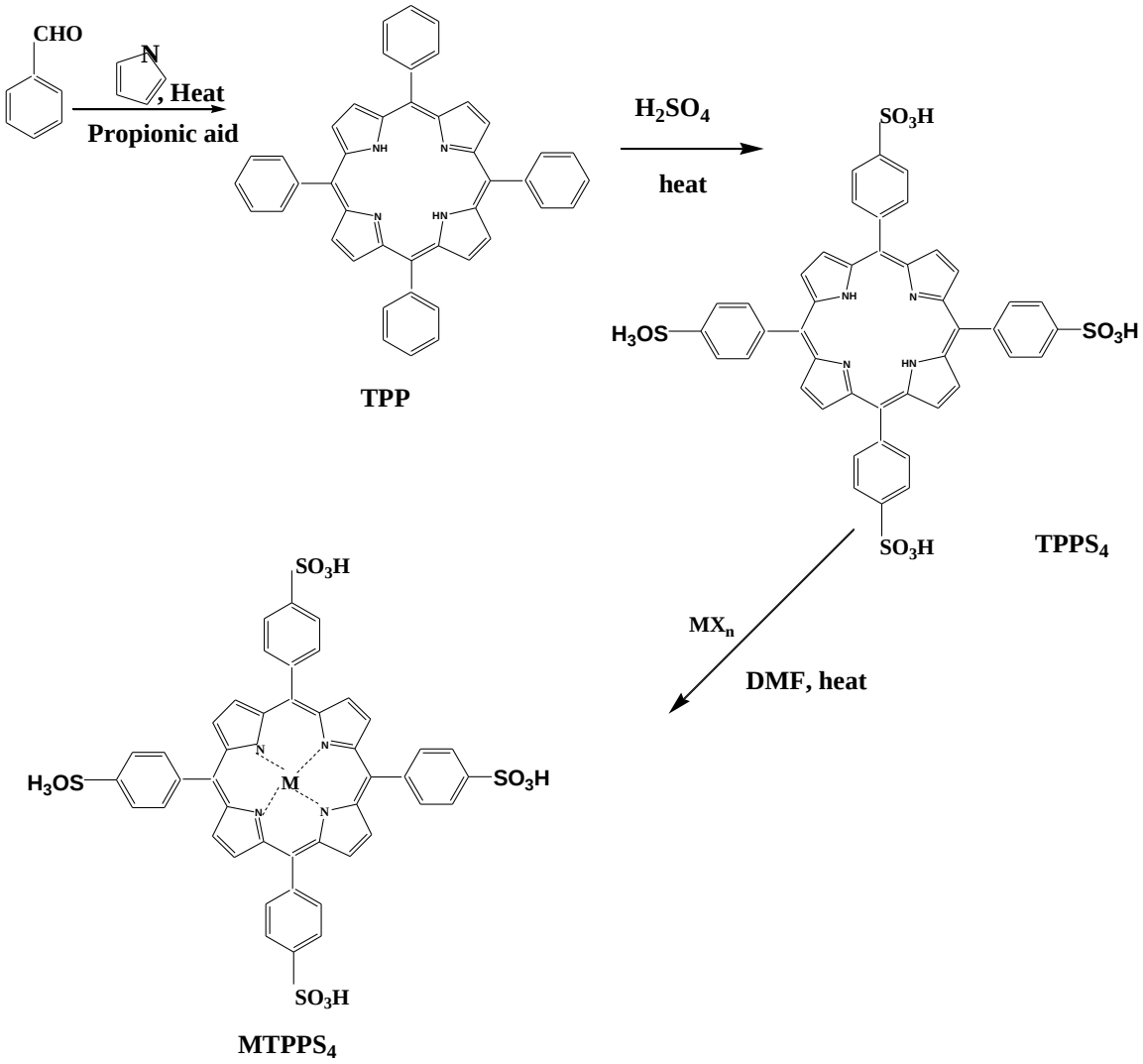

Scheme 2: Synthetic route of the meso-substituted porphyrin TPP, $TPPS_4$, and the corresponding metalloporhyrins where MX_n is a metallic salt.

1.1.3 Spectroscopic Characterization of Metalloporphyrins

Porphyrins are characterized by a conjugated structure of alternating single and double bonds. This feature creates chromogenic character in the visible and near infrared region. Porphyrins and their metal complexes generally exhibit characteristic sharp and intense absorption bands in the visible region. Unlike most transition metal complexes, the colour of metalloporphyrins is due to absorption(s) within the porphyrin ligand. The electronic absorption spectrum of a typical porphyrin consists of a strong transition (Soret band, B) and a weak transition (the Q band). The region from 400 to 500 nm, which is called the Soret band, shows the most intense absorption and molar extinction coefficient of the order 10^5 are often found [4]. The B and the Q bands both arise from $\pi \rightarrow \pi^*$ transitions and can be explained by considering the four frontier orbitals (HOMO and LUMO orbitals) (the so called Gouterman four orbital model) as per Figure 1.4.

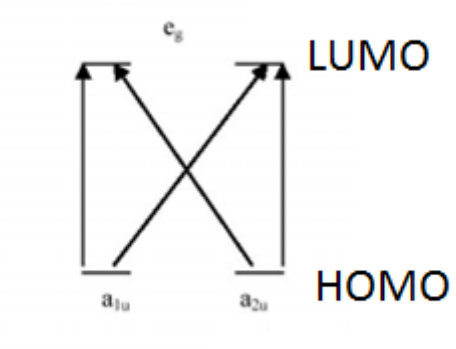

Figure 1.4 Orbital diagrams showing possible transitions for porphyrins.

According to Gouterman, the soret band originates from the a_{2u}, the highest occupied molecular orbital (HOMO) of the porphyrin to the e_{2g}, the lowest unoccupied molecular orbital (LUMO). This band is retained in the spectrum with significant modifications of the porphyrin macrocycle [6]. The Q band arises from a_{1u} to e_{2g}, thus it is a weaker transition. A typical absorption spectrum of a metalloporphyrin is shown in Figure 1.5.

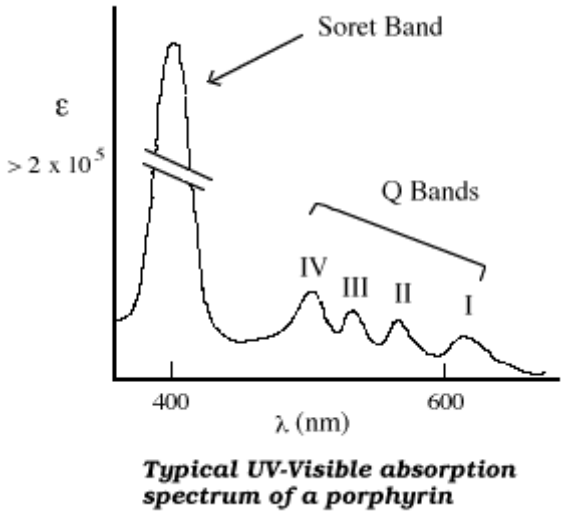

Figure 1.5 Typical absorption spectrum of a metalloporphyrin taken from [7].

Porphyrins can also be characterized by Emission spectroscopy as they have been found to be luminescent. Rapidly decaying luminescence is called fluorescence and it is a radiative decay from an excited state of the same multiplicity as the ground state. Internal conversion from second excited state to the first excited state is rapid so fluorescence is only detected from the first excited state. Generally, the porphyrins and their complexes emit in the region 500-700 nm.

Vibrational spectra of metalloporphyrins and related compounds have been studied extensively because of their biological importance as well as prosthetic groups of heme proteins. The typical spectra show that the bands between 1700 and 950 cm^{-1} are due to ν(CC), ν(CN), δ(CH), and δ(CCN) which are strongly coupled to each other. As a result, it is extremely difficult to assign band as they overlap [8].

1.1.4 Electrochemical properties of metalloporphyrins

Overview- Cyclic Voltammetry

Cyclic voltammetry is commonly used as an initial electrochemical technique to characterize a reduction/oxidation (redox) system. It is used to determine the half wave potential ($E_{1/2}$) and the number of electrons (n) transferred during the redox reaction. The solution of the species to be characterized is normally saturated with an inert gas, nitrogen or argon, in order to remove oxygen from the solution, as the presence of oxygen in the solution may interfere with the response of the species. In cyclic voltammetry, the potential is scanned linearly from an initial value E_i, to the second value E_f, and then back to E_i as per Figure 1.6. During the forward scan the species is reduced, resulting in a cathodic peak. When the scan direction is switched to the opposite direction the reduced species which has been accumulating near the electrode, is oxidized back resulting in an anodic peak. One or more potential cycles can be performed, hence the term "cyclic voltammetry".

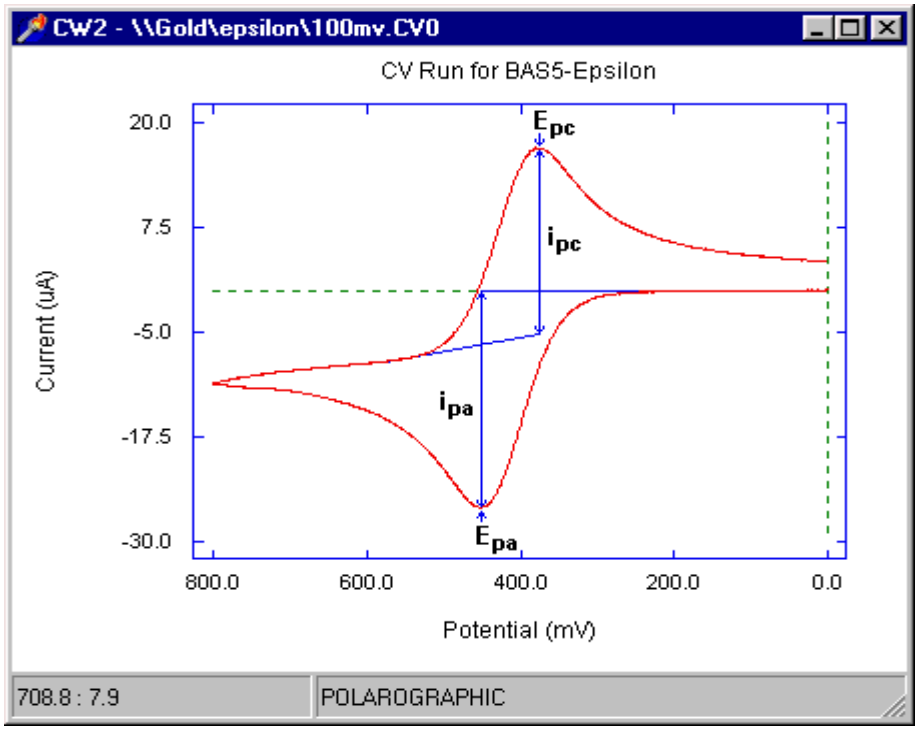

Figure 1.6 A typical cyclic voltammogram showing the important peak parameters

The important parameters for a cyclic voltammogram are the peak potentials E_p and peak currents i_p. If a redox system remains in equilibrium throughout the potential scan, the redox process is said to be reversible. The peak current ratio = i_{pa}/i_{pc} = 1 at all scan rates for a reversible process. For a one-electron process, the peak separation ΔE, should ideally be 0.058 V at 25 degrees Celsius and is independent of the scan rate (ν). The peak current i_p for the reversible system is described by the Randle-Sevcik equation for the forward sweep of the first cycle, eqn 1. The peak current function $i_p/\nu^{1/2}$ (ν = scan rate) is independent of ν.

$$I_p = 2.686 \text{ X } 10^5 \text{ n}^{3/2} \text{AcD}^{½} \nu^{½} \qquad (1)$$

Where n is number of electrons, A the electrode surface area, c the concentration of the electroactive species in solution and D the diffusion coefficient. According to Equation 4, peak current increases with the square root of scan rate ($\nu^{1/2}$) and is directly proportional to concentration for a reversible couple. The dependence of the peak current on $\nu^{1/2}$ is indicative of a diffusion controlled process. Electrochemical irreversibility is caused by a very slow electron exchange between the redox species and the working electrode. In a quasi-reversible system the anodic and cathodic peak current are reduced in size and the anodic and cathodic peak current ratio is not unity. Totally irreversible systems are characterized by a single oxidation or reduction peak without the return peak.

Electrochemical properties of metalloporphyrins

Since they are electron- rich systems, porphyrins and their metal chelates have very rich redox chemistry. Their electrochemistry is so complex because it depends on the type of solvent, the type of the porphyrin and/or the type of axially coordinated ligand [9]. Transition metalloporphyrins have been classified into redox inactive and redox active metalloporphyrins. The redox inactive metalloporphyrins have redox properties very similar to main group metalloporphyrins as the d metal orbitals do not lie within the

HOMO-LUMO gap of the porphyrin ring and the redox processes are expected to occur exclusively on the porphyrin ring. Zn(II) tetraphenyl (ZnTPP) is an example of the redox inactive metalloporphyin, where the redox processes occur exclusively on the porphyrin ring [10]. Electrochemical data reports for $RuTPPS_4$ and $RuTPPS_4$ is minimal and very brief reports available indicated that the oxidation and reduction of Ru and Rh metalloporphyrins occur on the porphyrin ring [11]. In this study, the electrochemical properties of the tetrasulphonatotetraphenyl porphyrins of Ru(III) and Rh(III) are explored.

1.1.5 Magnetic susceptibility of metalloporphyrins

The measure of the attraction to a magnetic field is called magnetic susceptibility. The mass magnetic susceptibility χ_{mass}, measured in $m^3 \cdot kg^{-1}$ in SI or in $cm^3 \cdot g^{-1}$ in CGS and the molar magnetic susceptibility (χ_{mol}) measured in $m^3 \cdot mol^{-1}$ (SI) or $cm^3 \cdot mol^{-1}$ (CGS) are defined by Equations 2 and 3 below, where ρ is the density in $kg \cdot m^{-3}$ (SI) or $g \cdot cm^{-3}$ (CGS) and M is molar mass in $kg \cdot mol^{-1}$ (SI) or $g \cdot mol^{-1}$ (CGS).

$$\chi_{mass} = \chi_v / \rho \qquad (2)$$

$$\chi_{mol} = M\chi_{mass} = M\chi_v / \rho \qquad (3)$$

When a material is placed in a magnetic field H, a magnetization (magnetic moment per unit volume) M is induced in the material which is related to H by $M = kH$, where k is called the volume susceptibility. Since H and M have the same dimensions, k is dimensionless. The net susceptibility of a paramagnetic substance χ_m^{corr}, is the sum of the paramagnetic and diamagnetic contributions, but the former almost always dominates. The χ_m^{corr} is related to the effective magnetic moment by the Equation 4

$$\mu_{eff} = 2.83 (\chi_m^{corr} .T)^{1/2} \qquad (4)$$

The number of unpaired electrons can be then be calculated using Equation 5

$$\mu_{eff} = \{4S (S + 1) + L (L+1)\}^{1/2} \qquad (5)$$

In the case where there is no orbital contribution i.e., L=0, μ_{eff} becomes $\mu_{s.o}$.

$$\mu_{s.o} = 4S\,(S + 1)^{½} \qquad (6)$$

where S is the spin angular momentum and is equal to n/2.

Different complexes may have in them a different number of unpaired electrons. Substances that have no unpaired electron orbital or spin angular momentum generally have negative values of χ_m and are called diamagnetic. These substances don't interact strongly with a magnetic field, and are in fact slightly repelled by a magnetic field. Their molar susceptibility varies only slightly with temperature. Substances with unpaired electrons, which are termed paramagnetic, have positive χ_m and show much stronger temperature dependence, varying roughly as 1/*T*. They will be strongly attracted to a magnetic field, primarily according to the number of unpaired electrons.

We can determine the magnetic susceptibility of a compound using a Gouy balance. A crude Gouy Balance is figure 2.1, on page 28. One places the sample in the test tube and adds masses to the pan to balance it out. The masses are recorded and the electromagnet turned on. If the sample is paramagnetic, the sample is attracted to the electromagnet. Masses are added to re-balance it. The difference in the masses (the apparent increase in the mass when the magnetic field is on is a measure of the sample's magnetic susceptibility) is used to calculate exactly how many electrons are in the outer shell and are unpaired. If the sample is diamagnetic, the sample is repelled from the electromagnet.

1.1.6 Applications of metalloporphyrins

Due to their strong absorption of light at around 400 nm, metalloporphyrins have gained the interest of scientists in physics, chemistry and medicine in the last two decades. They are well-known optoelectronic as well as biological materials and have been applied in physics as light-emitting diodes, magnets, non-linear optics and in medicine as photosensitizer in photodynamic therapy [12,13,14,15,16]. For instance, in the last three

decades, $TPPS_4$ (shown in Figure 1.7) and its water-soluble metallated sulphonated tetraphenyl porphyrins have been extensively studied and have been applied as tumour–localizing agents in Photodynamic therapy (PDT) [17]. This is the cancer treatment which uses light as illustrated in Figure 1.8.

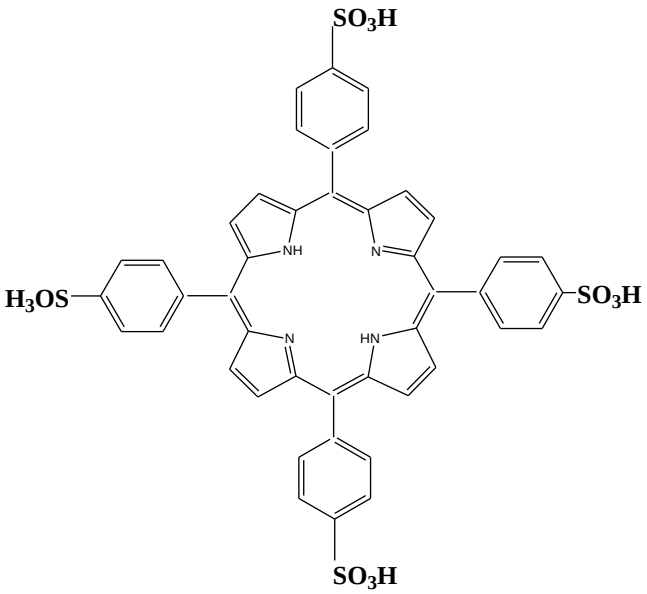

Figure 1.7: Chemical structure of tetrasulphonated tetraphenyl porphine ($TPPS_4$)

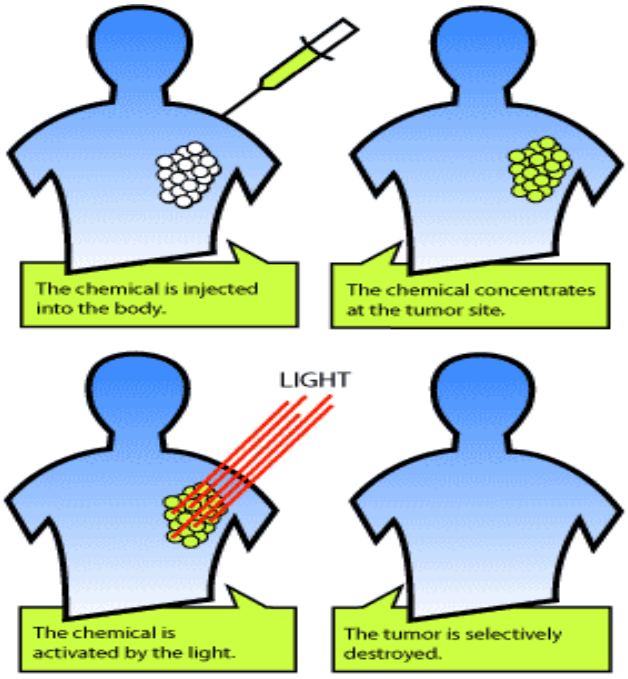

Figure 1.8 Illustration of the use of porphyrins in PDT.

In chemistry, they have been applied as sensors and catalysts [18, 19] and quite recently as homogeneous catalysts in oxidation reactions and polymerization reactions [20].

1.1.7 Catalytic Applications of Metalloporphyrins

Enzymes have been widely used in biochemistry, clinical chemistry and chemical engineering. Since their solutions are not stable under non-physiological conditions, study on their mimeses i.e. metalloporphyrins, is one of the interesting trends in chemistry. The development of new efficient catalysts has an important role in research. It is well known that some metalloporphyrins are very good catalysts, for instance, for the reduction of oxygen [21].

A reaction is not usually catalyzed by a unique species and a number of criteria must be considered when choosing the most effective catalyst, especially for a commercial process. Apart from change in reaction conditions that the use of a catalyst may bring about for example pressure and temperature, other factors that must be considered are the concentration of a catalyst, the catalytic turnover, the selectivity of the catalyst and how often the catalyst needs renewing. In general, for a metalloporphyrin to be applied as a suitable homogeneous catalyst, it must satisfy certain important requirements. The metalloporphyrin must be oxidatively stable and must be capable of forming complexes of varying coordination numbers and geometry. It must be capable of being "tailor-made" for selective oxidation and where possible, be reusable.

The noble metals otherwise known as the Platinum Group Metals (PGMs) which include ruthenium, osmium, rhodium, iridium, palladium, platinum, silver, and gold and they form a variety of complexes M(P) LL′ with tetrapyrrole ligands which are studied in many laboratories because their coordination chemistry and catalytic power is similar to that of the corresponding iron and cobalt tetrapyrroles forming the prosthetic groups in heme proteins and vitamin B_{12} [22]. Extensive studies have been carried out with

metalloporphyrins of Fe(II), Mn(II) and Co(III) TPyP's to polymerize aniline by Nabid *et al*. These water-soluble metalloporphyrins mimic the various reactions of horseradish peroxidaze (HRP) and other monooxygenases in different reactions [23]. The reaction of aniline derivatives with hydrogen peroxide catalyzed by oxidoreductase is a route to the synthesis of industrially important polyaromatics. Horseradish peroxidase and related enzymes show low stability under nonphysiological conditions, whereas metalloporphyrins are more stable and more promising for catalytic polymerization of aniline.

1.2 Polyaniline

Polyaniline (PANi) is a polymer of aniline. The monomer aniline, Figure 1.9 (a) was obtained for the first time from the pyrolytic distillation of indigo and was called "Krystallin" because it produced well formed crystalline salts with both sulfuric and phosphoric acid. In 1840, Fritzsche also obtained colorless oil from indigo, called it aniline and oxidized it to polyaniline [24].

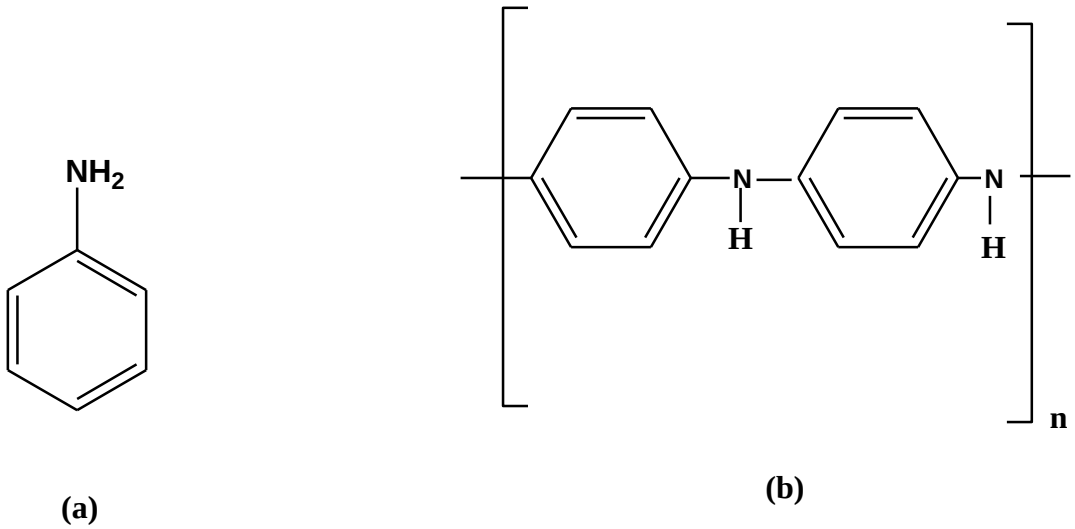

(a) **(b)**

Figure 1.9 Chemical structure of Aniline (a) and Polyaniline (b); where n is the chain length

Polyaniline is a phenylene-based polymer having –NH group on either side of the phenylene ring. It is one of the most studied conducting polymers of semi-flexible rod polymer family [25]. Conducting polymers (CP's) represent a class of polymers possessing the π-conjugation system with continuous mobile π-electrons, and can be characteristically reduced or oxidized reversibly [26]. These conducting polymers are often termed organic metals. Among these CP's, PANi has gained relatively high popularity. According to Web of Science, more than 10,000 papers appeared in the past 30 years on various aspects of chemistry, physics and engineering of this polymer [27]. Unlike other conjugated polymers, PANi has been widely studied due to its several advantages over other conducting polymers. The raw materials are cheap and easily available and the synthetic routes are easy. PANi has good environmental stability, simple and reversible

acid/base doping/dedoping chemistry which enables control over properties such as free volume, solubility, electrical conductivity and optical activity and interesting electrochemical properties which are associated with the chain nitrogen [28,29]. The oxidation and reduction occur on the –NH group, and various oxidation states are obtained due to the number of imine and amine segments on the PANi chain.

Due to these amazing properties, PANi is used as filler in the preparation of conducting composites, and for the surface modification of microparticles, powders, fibers, textiles, membranes, and porous substrates, endowing them with new electrical, chemical, and surface properties. The changes in the physicochemical properties of PANi occurring in response to various external stimuli are used in various applications, e.g. in electrodes, sensors, and actuators. Some applications are based on the combination of electrical properties typical of semiconductors with materials parameters characteristic of polymers, like the development of "plastic" microelectronics and "smart" fabrics [30,31].

Polyaniline can be found in three idealized oxidation states shown in Figure 1.10. These redox states are leucoemeraldine, emeraldine and pernigraniline.

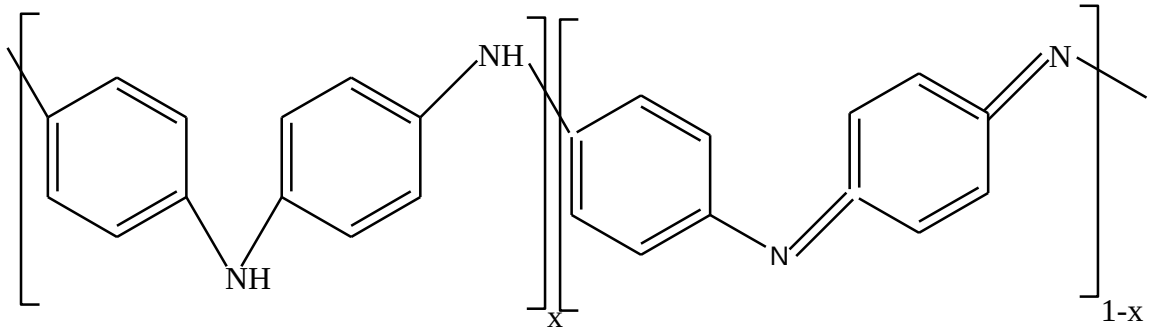

x =1: Leucomeraldine
x = 0.5: Emeraldine
x = 0 : Pernigraniline

Figure 1.10 Different oxidation states of PANi, where x is the degree of polymerization

Leucoemeraldine is the fully reduced state while Pernigraniline is the fully oxidized state with imine links instead of amine links. The emeraldine form of polyaniline, often referred to as emeraldine base (EB), is either neutral or doped, with the imine nitrogens protonated by an acid. In strongly acidic medium, the imine nitrogens are protonated yielding corresponding polyaniline salt forms: fully reduced leucoemeraldine salt (LES, x = 1), semi-oxidized emeraldine salt (ES, x $\sim$ 0.5) and fully oxidized pernigraniline salt (PNS, x = 0). Emeraldine base is regarded as the most useful form of polyaniline due to its high stability at room temperature and the fact that upon doping the emeraldine salt form of polyaniline is electrically conducting. It must be noted that the fully reduced and fully oxidized forms are poor conductors, even in the presence of a dopant acid. The potential ranges of existence of these forms depend on the composition of the electrolyte. Both the cations and the anions contribute to maintaining the charge neutrality inside the polymer.

1.2.1 Why it is conducting?

Emeraldine form of polyaniline is conducting because of the small band gap. In solids, there are two energy bands: valence band and conduction band as shown in Figure 1.11. The energy spacing between these two bands is called the band gap and this gap is significantly large in insulators. Semiconductors have an electronic structure similar to that of insulators, but with a small band gap. Electrons can be excited into the conduction band, making semiconductors somewhat conductive at room temperature. Electrons in the conduction band conduct electricity as does the empty state in the valence band, corresponding to a missing electron (hole) in one of the covalent bonds as shown in the simplified band diagram Figure 1.11.

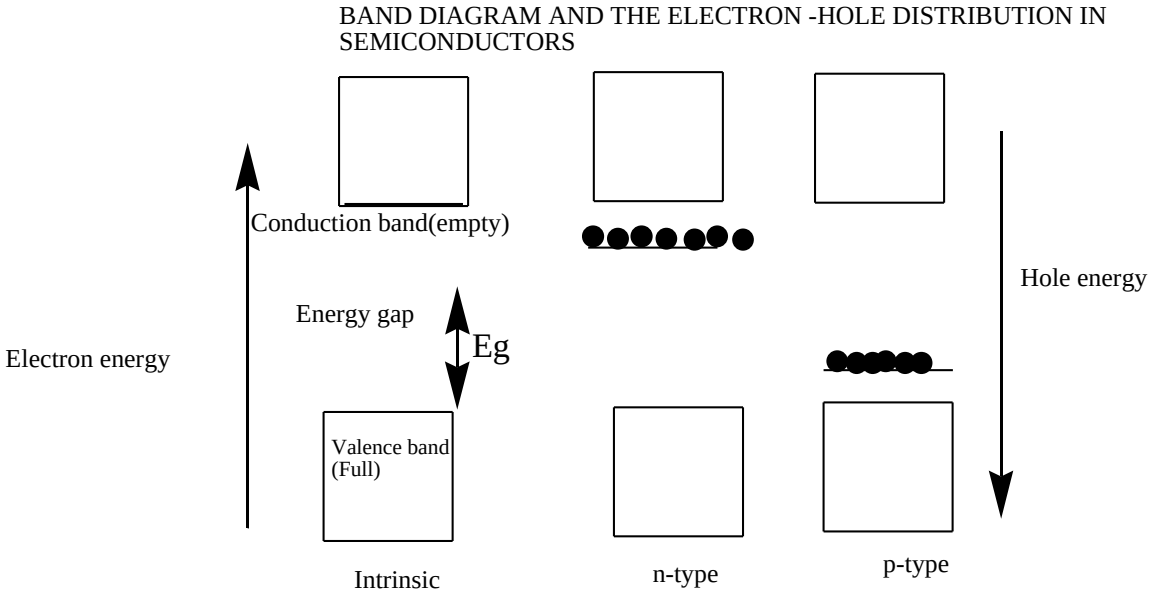

Figure 1.11 Band diagram and the electron hole distribution in semiconductors.

1.2.2 Synthetic Routes for PANi

PANi can be synthesized either chemically or electrochemically in acidic solutions. The chemical route is simple, inexpensive and the route of choice for bulk production. Chemical synthesis entails the oxidative polymerization of the monomer in an acidic medium using strong oxidants such as hydrogen peroxide, ammonium persulphate, potassium persulphate, potassium dichromate or ferric ions in the presence or absence of templates. Although the synthetic methods to produce polyaniline are quite simple, its mechanism of polymerization and the exact nature of its oxidation chemistry are quite complex. The reaction mechanism proposed by Bejan and Duca for the polymerization of anilines and aniline related monomers is similar [32]. The oxidants are able to oxidize the monomer leading to chemically active cationic radicals. The cationic radicals then react with more monomer molecules producing a polymer.

For the purposes of this study, only chemical and enzymatic polymerization will be reviewed. No matter which synthetic route is taken, PANi has poor processability due to stiff backbone. This is due to the aromatic nature and intermolecular hydrogen bonding between amine groups (donors) and imine's groups (acceptors) of the adjacent chain. The

morphology and processabilty of PANi were found to vary mainly with chemical nature of oxidant, synthetic pathway, temperature at which the reaction is carried out, the presence and nature of a dopant, the presence and nature of a template and the presence or nature of a catalyst.

It is therefore claimed that there are as many types of PANi as there are people who synthesized it because of these factors [33]. For instance polymerization of aniline carried out in aqueous medium using an oxidant and protic acid results in highly unprocessable PANi. Tremendous efforts or attempts have been made during the last two decades to make use of this important polymer. Osterholm *et al.* have adopted emulsion polymerization pathway to prepare processable conducting PANi in the presence of dodecyl benzene sulphonic acid (DBSA) and ammonium persulphate (APS) as the oxidant [34]. The authors claimed the improved solubility was attributed to enhanced homogeneous protonation by DBSA. Later Kinel *et al.* followed a slightly different route in that they used a biphasic system i.e., water immiscible dinonylnaphthalene sulphonic acid (DNNSA) and APS as the oxidant [35]. PANi prepared was soluble in most organic solvents. Pillai *et al*. have reported the use of sulphonic acid of 3—pentadecylphenol (SPDP), 3-pentadecylanisole (SPDA) and 3-pentadecylphenoxic acid (SPDPAA) as dopants to produce a conducting PANi. These dopants act as plasticizing cum protonating agents [36].

Palaniappan *et al.* have synthesized a highly processable and conducting (2.53 S cm^{-}) PANi using benzoyl peroxide (BP) as a novel oxidant, sodium lauryl sulphate as a surfactant in the presence of sulphosalicylic acid while a similar experiment using APS produced a less conducting PANi (2 X 10^{-2} S cm^{-1}) [37]. Shreepathi and co-workers have reported a new emulsion pathway for the synthesis of soluble PANi using BP as the oxidant in 2-propanol/water solvent system. DBSA served as the dopant and surfactant. Authors achieved complete solubility in chloroform and 2:1 toluene/ 2-propanol mixture without leaving any solid residues [38]. Bicak *et al.* have also demonstrated a different approach to synthesize soluble PANi using oxygen as the oxidant in the presence of Copper(II) nitrate which acted as the catalyst in a biphasic system (water/chloroform).

The reaction was reported to take place in weakly basic and neutral medium. Authors suggested that under these conditions, the coupling via ortho positions was restricted hence the solubility was improved [39].

As mentioned, PANi offers great applicability potential in various fields but its application is hindered by its insolubility and infusibility. Derivatization of PANi by introduction of functional moieties within the benzene ring or imine nitrogens has been done. For instance, Iwuoha *et al*. have reported a highly soluble conducting PANi doped with Anthracene Sulphonic Acid (ASA) [40] while Nabid *et al*. have proposed that anionic metalloporphyrins of Fe, Co, and Mn catalyse the polymerization of aniline resulting in a green soluble PANi [41]. Extensive studies have been carried out with tetrapyridylporphyrins (TPyP) and phthalocyanines of Fe (II), Mn (II) and Co (II) to polymerize aniline by Nabid *et al*. by the mechanism shown in Scheme 3 [23] . The polymerization of aniline by metalloporphyrins in aqueous acidic solutions and in the presence of a strong polyelectrolyte, SPS (poly (sodium 4-styrene sulphonate)), produced the water-soluble and conducting form of polyaniline. As is shown in Scheme 3, after the addition of hydrogen peroxide to the solution of FeTPyP, iron (III) hydrogen peroxide porphyrin complex [(TPyP)FeIII–OOH] was formed. This is due to the fact that the Fe(TPyP)Cl complex tends to form a high-valent iron (IV) oxo porphyrin cation radical intermediate [(TPyP) + Fe=O], via O–O bond heterolysis in the reaction between iron porphyrin complex with H_2O_2. Then, the intermediate reacts with aniline, resulting in the aniline cation radical. This cation radical attacks other cation radicals of the monomer to form a dimer, by eliminating two hydrogens. The reaction further propagates to give PANi.

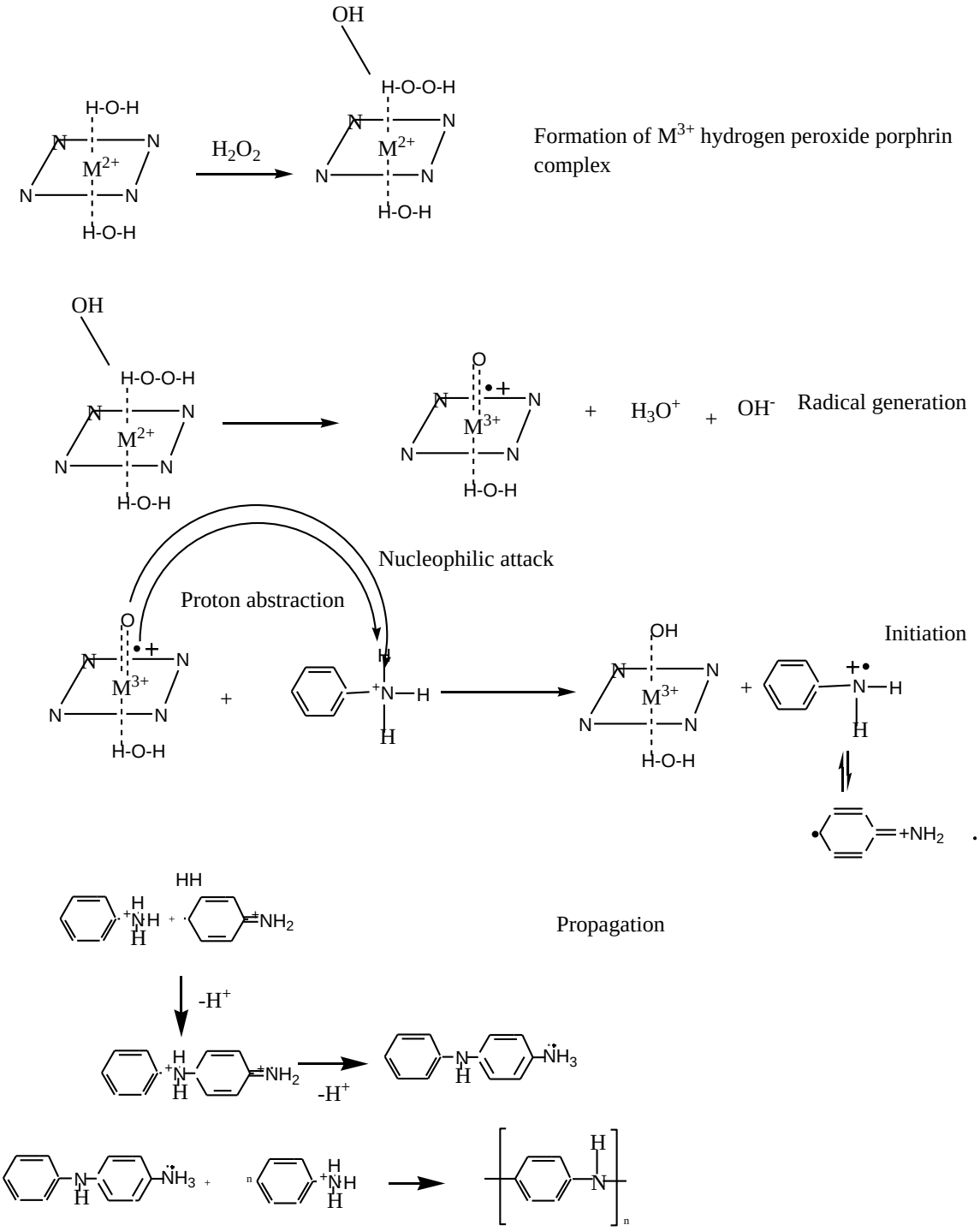

Scheme 3: Proposed mechanism for metalloporphyrin catalyzed polymerization of aniline

The water soluble tetrapyridylporphyrins of Fe, Co and Mn mimic the various reactions of horseradish peroxidase (HRP) and other monooxygenases in different reactions. In industries, the reaction of aniline and its derivates with hydrogen peroxide catalysed by oxidoreductase is a synthetic route for the synthesis of industrially important polyaromatics. HRP and related enzymes show poor stability under non-physiological conditions, whereas metalloporphyrins are more stable, relatively cheaper and more promising for catalytic polymerization of aniline. According to the reviewed literature, metalloporphyrins of Platinum Group Metals (PGMs) have not been used for this particular process. In the available literature reviewed for this study, different ways to produce processable PANi have been demonstrated and are summarized in Table 1.

Table 1: A summary of synthetic methods for processable PANi.

Synthetic method and experimental conditions	Conductivity S cm^{-1}	Stability	Processability	Reference
Copolymerization				
-PSA	-moderate	-Good	-Good	[42]
-ASA	-moderate	-Good	-Water soluble	[40]
Emulsion polymerization				
-DBSA/APS/Water/	-Moderate	-Good	-Good	[34]
-DNNSA/Water	-Good	-Good	-Soluble in organic solvents	[35]
-SPDPPA/Water	-Good	-Good	-Poor	[36]
-DBSA/ 2-propanol-Water				
-APS	-2.53	-Good	-moderate	[37]
- BP	-2 $x10^{-2}$	-Good	-soluble in $CHCl_3$ and 2:1 toluene/2-propanol	[48]
$-O_2/Cu(NO_3)_2$/Water-$CHCl_3$				
-PTSA	-0.28	-Good		[39]
-DBSA	-0.32	-Good	-Moderate -Moderate	[39]

PANi Composites/Blends -PANi/carboxylated PVC	-7 x 10^{-2}	-Good	-Good	[43]
Self Assembly -MABSA on Indium Tin Oxide (ITO)	-Moderate	-Good	-Good	[44]
Metathesis Polymerization p-dichlorobenzene and sodium amide in benzene, 220°C	-Good	-Good	-Water-soluble	[45]
Catalysed Polymerization -Enzymatic-HRP -SYP -Metal complexes -Pthylocaynines(Fe,Co,Mn) -Anionic Porphyrin (Fe,Co,Mn) -Cationic (Fe,Co,Mn)	 -Good -Good -Moderate -Moderate -Good	 -Good -Good -Good -Good -Good	 -Water soluble -Water soluble -Water soluble -Water soluble -Water soluble	 [46] [47] [41] [41] [23]

1.3 Objectives of the Study

No matter which synthetic method is used to prepare PANi, it has poor processability both in melt and solution forms due to its stiff backbone and insolubility in most organic and inorganic solvents [48] . In this work, we employ a unique approach which we hope will address and almost resolve the current limitations of both the enzymatic and the chemical routes for synthesis of PANi. We employ metalloderivatives of sulphonated porphyrins of Ru(III) and Rh(III).The method consists of using anionic template (SPS) which is believed to promote the head to tail coupling of aniline radicals and enhance solubility in water. The detailed objective of the research in this study is to synthesize and characterize water soluble metalloporphyrins i.e. Ruthenium (III) tetrasulphonated tetraphenyl porphyrin ($RuTPPS_4$) and Rhodium (III) tetrasulphonated tetraphenyl porphyrin ($RhTPPS_4$) and to explore the catalytic behaviour of these complexes towards polymerization of aniline. We would like to explore the mechanism for the interaction of the monomer (aniline) and the catalyst and lastly, to compare the effect of the metal centre towards the catalysed synthesis of Polyaniline.

1.4 Outline of Thesis

This thesis contains five (5) chapters. The first chapter provides background information on the metalloporphyrins, their synthetic routes and applications especially in catalysis. A literature review on the synthetic routes towards a more processable and conducting PANi and the objectives of this study are also discussed in the first chapter of the thesis. Chapter two describes synthetic methods and instrumentation that were used throughout the whole research. Chapter three presents the results of synthesis of metalloporphyrins and their characterization. The catalytic capabilities of the selected metalloporphyrins in polymerization of aniline using hydrogen peroxide as an oxidant is investigated and also described in this chapter. Studying the main factor responsible for catalysis is considered in this chapter. Finally, the last chapter represents the conclusion of this research and provides a summary of the results and potential avenues for future research.

CHAPTER 2

EXPERIMENTAL: METHODS AND INSTRUMENTATION

2.1 Synthesis of the Metalloporphyrin Complexes

2.1.1 Preparation of meso-tetrakis (4 –sulphonato) porphyrin- $TPPS_4$

Meso-tetrakis (4 –sulphonato) porphyrin was prepared by direct sulphonation of meso-tetraphenyl porphyrin TPP following the literature method of Busby *et al.* [49]. Tetraphenyl porphyrin that was used as a precursor was synthesized in our laboratory following the method of Adler *et al.* [50]. Sulphonation of TPP was achieved by suspending 3.0 g (4.90×10^{-3} mol) of TPP in concentrated sulphuric acid (75 mL) in a 250 mL round bottomed flask equipped with a drying tube filled with $CaCl_2$ as a drying agent. Care must be taken as dissolution of TPP in concentrated sulphuric acid is exothermic. The green solution was refluxed for 9 hours at 150°C. The product was purified by first performing dialysis using dialysis tube (Merck, molecular weight cutoff = 500) and then column chromatography with the use of Alumina of the second degree of activity (UniLAB) employing distilled water as the mobile phase. Completion of sulphonation was confirmed by UV-Vis Spectroscopy as shown in Table 3.1. Yield (72%).

2.1.2 Synthesis of $RuTPPS_4$ and $RhTPPS_4$

Synthesis of $RuTPPS_4$ was achieved by refluxing the $TPPS_4$ (0.12 g, 1.28×10^{-4} mol) with analytical grade Ruthenium chloride trihydrate (0.02 g, 5.79×10^{-4} mol) (Merck) in weakly coordinating DMF (Merck) for about 8 hours at temperatures around 200 °C, following the method of Kubat [51]. The purity of the metalloporphyrins was confirmed by thin-layer chromatography. Yield 64.3%. The same procedure was followed for synthesis of $RhTPPS_4$; but 0.02 g (7.60×10^{-5} mol) of Rhodium chloride trihydrate was used, instead of $RuCl_3.3H_2O$.Yield 60.4%.

2.2 Preparation of reagents

A hot solution of sodium perchlorate (1.0 M, 100ml) and tetraethylammonium chloride (Sigma) was mixed and the mixture was cooled in ice cold water. The precipitate formed was filtered, washed with ice cold ethanol (95 %) and TEAP recrystallised from ethanol (95 %). TEAP thus obtained was dried in the oven overnight and used as an electrolyte in electrochemical experiments in non aqueous solvents. Yield, 80 %.

2.3 Instrumentation

Electronic absorption spectra were recorded with a Shimadzu UV-1201 spectrophotometer. Baseline correction was done prior the measurements of the samples. Quartz cuvettes of 10 mm path length were used. Emission spectra were recorded on a Shimadzu RF-1501 spectrofluorometer. The excitation wavelength was set at 400 nm. Infrared spectra were recorded on a Magna-IR 760 spectrometer (Nicolet) in pre-dried KBr mull in the 4000-400 cm^{-1} region. Correction for both H_2O and CO_2 was made prior the measurements of the sampes.

Electrochemical data was collected using a BAS model CV- 100W electrochemical analyzer (BASi, Lafayette, USA) in both aqueous and non-aqueous media. All measurements were carried out under an atmosphere of purified nitrogen. In non aqueous medium, predistilled DMF was used as the solvent with TEAP (own synthesis) as the supporting electrolyte. Sodium sulphate was recrystallised from ethanol and was used as a supporting electrolyte in aqueous medium. In all electrochemical experiments standard three electrode operational amplifier circuitry was used. The glassy carbon (d = 1.6 mm) served as the working electrode in aqueous medium while the platinum disc (d = 1 mm) was used in non aqueous medium. The platinum wire served as the auxiliary electrode. The electrochemical measurements were done against the Ag/AgCl in non-aqueous medium while the reference electrode for aqueous medium was SCE. Highly pure nitrogen was passed through the electrolytic cell prior to measurement. All solutions were stored in the darkness. It followed from the spectrophotometric study that the stock solution was stable for at least 240 days [52].

The magnetic susceptibility measurements were determined using a 50.5mT Metter Gouy balance (schematic representation -Figure 2.1) at 20°C. The mass of the empty tube with and without field was weighed and recorded. $CuSO_4.5H_20$ was used as the calibrant. Masses of the samples ($RhTPPS_4$ and $RuTPPS_4$) were also measured with and without field. The mass of water without field was also measured and recorded.

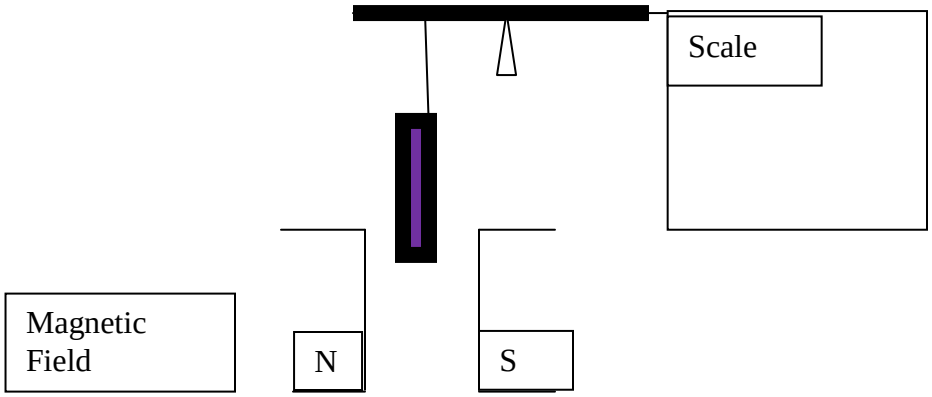

Figure 2.1: Schematic representation of a Gouy Balance

2.4 Synthesis and Characterization of PANi

The polymerization of aniline with hydrogen peroxide catalyzed by water-soluble transition-metal sulphonated tetraphenyl porphyrin at ambient temperature was done according to the method described by Nabid *et al.* [23]. Under constant stirring, 1 g (4.85 mmol) of SPS and 5 ml (9.17×10^{-2} mol) of aniline were added to a 100 ml conical flask containing 2 ml strong acidic solution of pH 2. After that, 2.5 ml (3×10^{-5} M) of the $RuTPPS_4$ was added to the mixture. The reaction was initiated by adding 4.5 ml (0.02 M) of diluted hydrogen peroxide under vigorous stirring. The polymerization continued for 72 h in a closed vial (parafilm). The final bluish-green solution was dialyzed (molecular cutoff = 1000) overnight to remove any unreacted catalyst, monomers and oligomers. Other catalyst ($RhTPPS_4$) was employed using the same method to polymerize aniline. The polymers were then characterized by FTIR, UV-Vis spectroscopy. The redox behaviour of the polymers was studied in 1M HCl on a platinum electrode.

CHAPTER 3

3.0 RESULTS AND DISCUSSION

3.1 Synthesis of metalloporphyrins

The preparation of $RuTPPS_4$ was carried out by refluxing mesotetrakis (4-sulphonato) phenyl porphyrin ($TPPS_4$) with $RuCl_3.3H_2O$ salt as shown in Scheme 4. The method of preparation is outlined in section 2.1.1.

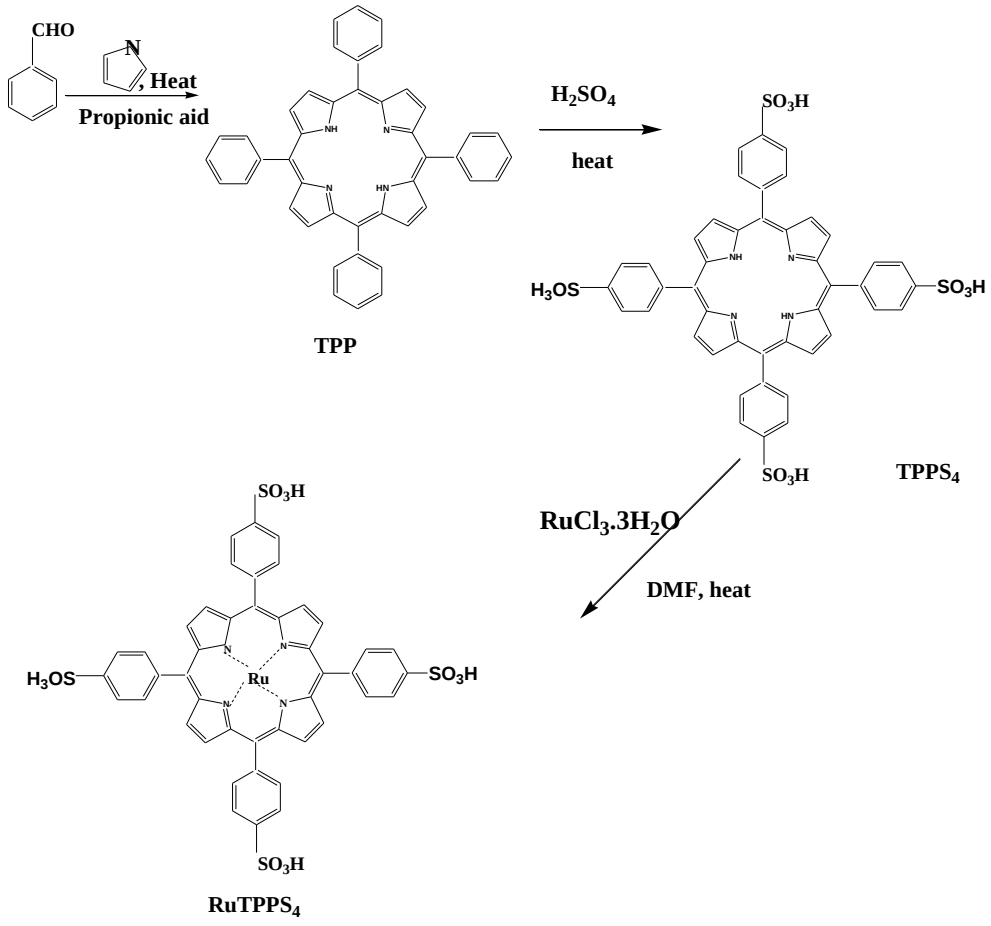

Scheme 4: Synthesis of $RuTPPS_4$

Rhodium (III) mesotetrakis (4-sulphonato) phenyl porphyrin was synthesized following the same scheme but $RhCl_3.3H_2O$ was used instead of $RuCl_3.3H_2O$.

3.1.1 Absorption Spectroscopy

Mesotetrakis (4-sulphonato) phenyl ($TPPS_4$)

TPP was insoluble in water hence its spectrum was recorded in ethanol. Sulphonation rendered it water soluble. Figure 3.1 shows the electronic absorption spectra of TPP in ethanol and $TPPS_4$ and they both comprise the (π -π^*) absorption bands characteristic of free-base type porphyrin. For TPP, an intense near-UV Soret band (SB) is located at 421 nm. In $TPPS_4$, the soret band is located at 435 nm indicating bathochromic (red) shift of 14 nm. This red shift can be attributed to sulphonation of TPP. This is due to the electron withdrawing effect of the sulphonato substituent on the phenyl groups. The Q bands were not observed in the spectrum of TPP in the region 500-700 nm. For $TPPS_4$, the Q bands in the visible spectral region are located at 483 nm, 579 nm, 592 nm and 636 nm. The spectrum of free porphyrin and sulphonated porphyrin were notably different and this confirmed that sulphonation process had occurred.

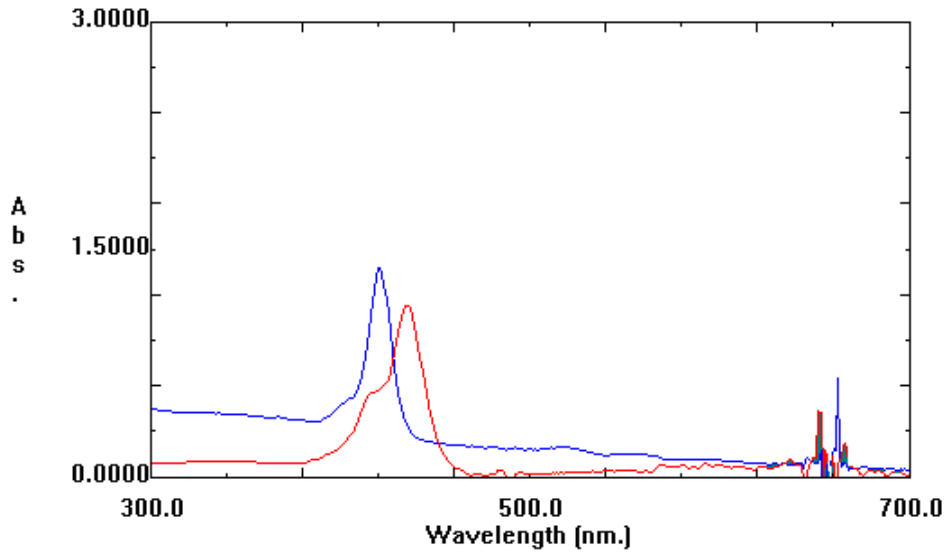

Figure 3.1: Electronic Absorption spectrum of TPP in ethanol (blue) and TPPS4 (red)

Upon insertion of the metal, the soret band shifted to lower wavelengths with a greater shift in Ruthenium complex than in Rhodium complex as per figure 3.2. The soret band for $RuTPPS_4$ is located at 388 nm and that of $RhTPPS_4$ at 419 nm.

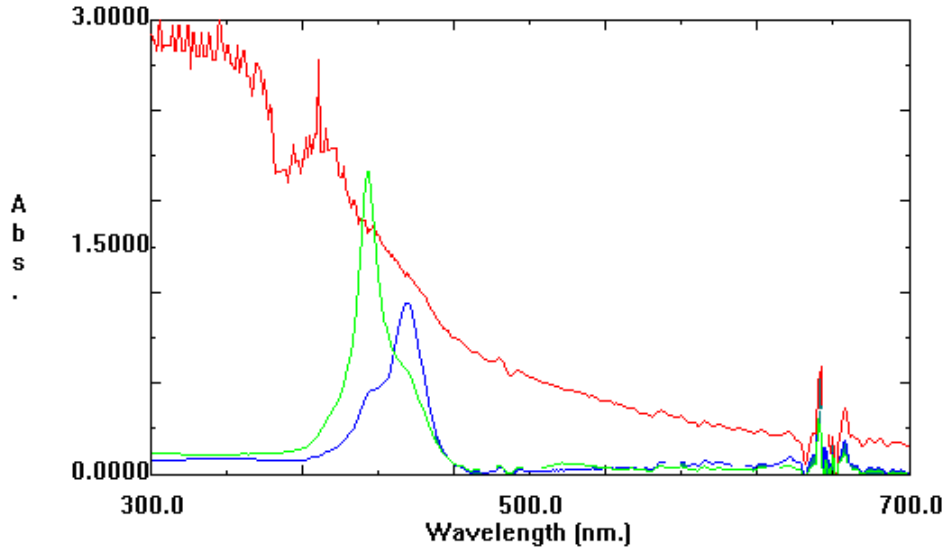

Figure 3.2: Electronic Absorption spectrum of $TPPS_4$ (blue), $RhTPPS_4$ (green) and $RuTPPS_4$ (red)

The observed shift of the soret band could be attributed to the larger size of ruthenium as it just sit on top of the macrocyclic, distorting the geometry further [53]. The soret band in $RuTPPS_4$ was observed to nearly overlap with the charge transfer bands. Ru (III) has an electron configuration of $[Kr]4d^5$ hence it can accept electrons from electron rich porphyrin ligand in its half-filled subshell. These are called Ligand to Metal Charge Transfer bands (LMCT) as shown in Figure 3.3. The LMCT bands are of high energy, and both spin and Laporte allowed, hence they have very high intensities. Table 3.1.shows the electronic absorption data for $TPPS_4$, $RuTPPS_4$ and $RhTPPS_4$ complexes.

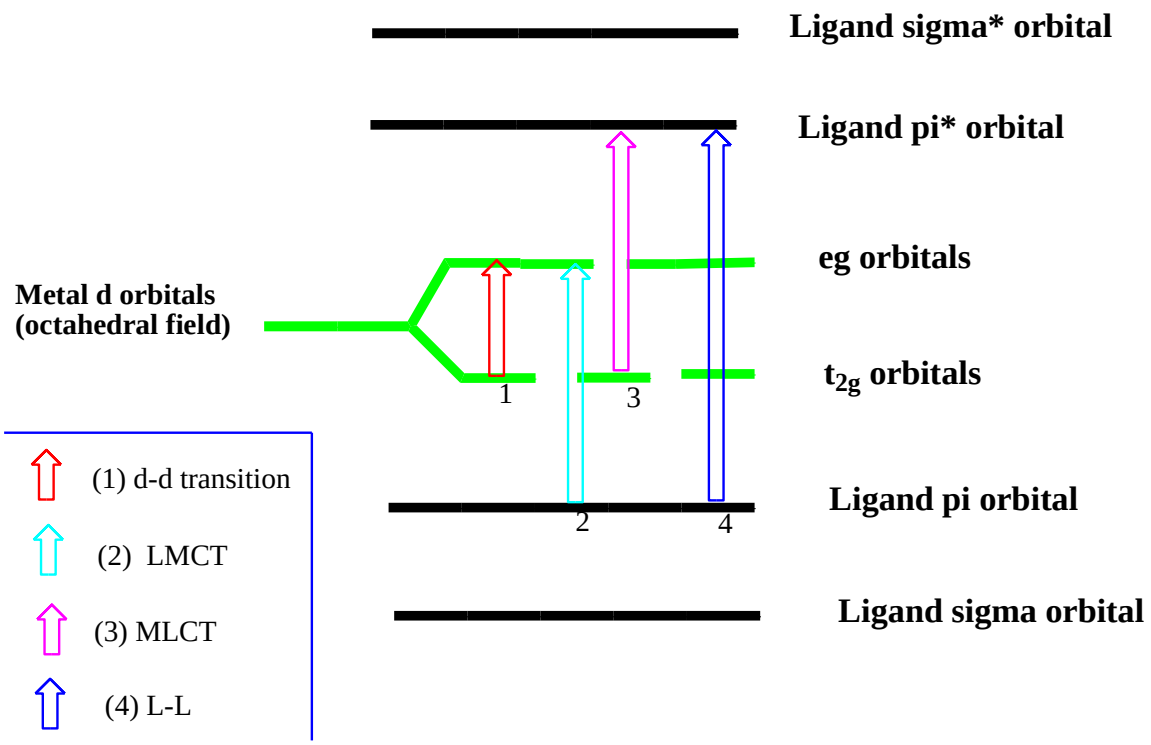

Figure 3.3: Light absorption in d-block (octahedral) complexes resulting in from left: metal centred transition (MC), ligand to metal charge transfer (LMCT), metal to ligand charge transfer (MLCT) and ligand-ligand transition (L-L).

Table 3.1: Electronic Absorption data for studied porphyrins.

Compound	λ1 nm	λ2 nm	λ3 nm	λ4 nm	λ5 nm	λ6 nm
TPP	515	421	_	_	_	_
$TPPS_4$	652	592	423	336	_	_
$Rh(TPPS_4)$	666	635	579	519	483	419
$Ru(TPPS_4)$	666	636	622	569	494	388

3.1.2 Emission Spectroscopy

Figure 3.4 shows the fluorescence spectra of TPP in ethanol and $TPPS_4$ in water. Excitation was made at 400 nm because at that wavelength, a large fraction is predominantly absorbing thus gives rise to a larger quantum yield.

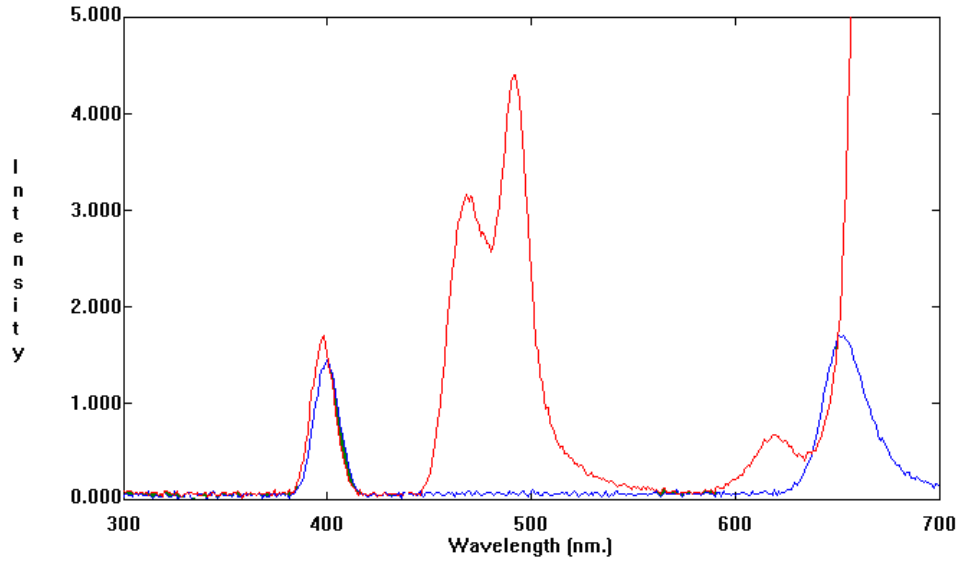

Fig.3.4: Fluorescence spectrum of TPP in ethanol (blue) and $TPPS_4$ in aqueous solution (red).

The excitation peak of $TPPS_4$ in aqueous solution is sharper, and blue-shifted by 4 nm in comparison to TPP in ethanol. This could be due to solvent effect. Sulphonation of TPP also caused the blue shift of the main fluorescence maximum by 28 nm and appearance of the second fluorescence peak at about 488 nm. This peak splits into two components which is indicative of formation of aggregates. The absorption band of J-aggregates is at 488 nm and is in agreement with literature data [54]. The formation of aggregates was also indicated by an increased intensity of the band at around 700 nm [55]. The aggregates formed in neutral solution show only one structureless emission band at 664 nm due to the (0-0) transition. Some authors suggested that $TPPS_4$ does not stack in water [56] since the negative charges at the sulphonato groups cause the electrostatic repulsion between $TPPS_4$ molecules however our experimental results clearly support the assumption that

the dimerization equilibrium exists for $TPPS_4$ as an intense structureless emission band and splitting of the band were observed.

Nevertheless, it is difficult to expect that the negatively charged sulphonato groups of $TPPS_4$ would tend to be located in close proximity in the face-to-face dimer, keeping in mind the fact that phenyl groups are nearly perpendicular to the plane of porphyrin ring in non-protonated species. Then the favourable structure for a face-to-face dimer of $TPPS_4$ could be such that both steric constraints induced by out-of-plane sulfonatophenyl groups and electrostatic repulsion of negative charges localized on the sulfonato group are minimized by 45° rotation of one monomer with respect to each other. The negative charges of the peripheral sulphonato- groups do have a strong effect on the distribution of the electronic density near nitrogen atoms of a tetrapyrrolic macrocycle. As a result, a charge transfer state may be formed due to interactions between negatively charged substitutes of one porphyrin monomer and the nitrogen in the center of other monomer. This can lead to stronger van der Waals interaction for a face-to-face dimmer [57].

The emission data of the synthesized complexes are shown in Figures 3.6 and 3.7. The fluorescence intensity in $RuTPPS_4$ and $RhTPPS_4$ is lower when compared to the intensity of $TPPS_4$. This fluorescence quenching of the complexes could be attributed to an electron transfer from the singlet excited state (S_1) of the $TPPS_4$ to the complex moiety. Ruthenium complex absorbs at 404 nm and emits most strongly at 685 nm and weakly at 482 nm in deaerated water while Rhodium complex emits weakly at 690 nm. For the ruthenium complex, these emissions are caused by radiative process from ^{3}LMCT state to the ground state (GS) and ^{1}LMCT state to the GS [58]. These radiative processes are called Phosphorescence and Fluorescence respectively and they can be explained with a simplified Jablonski diagram for the inorganic complexes, Figure 3.5. Due to incorporation of metal orbitals, the Jablonski diagram needs to incorporate the notation discussed.

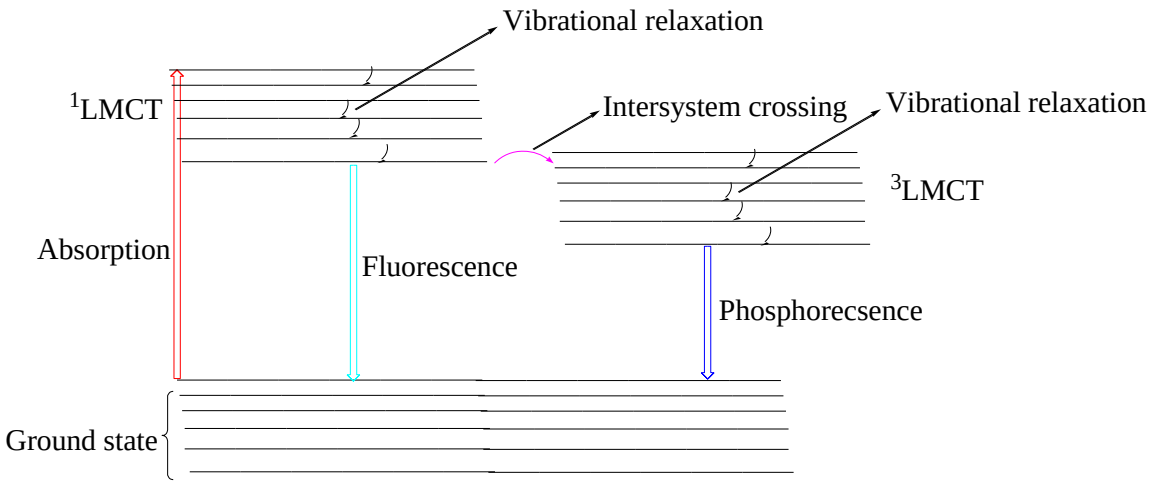

Figure 3.5 Proposed Partial Jablonski diagram for the Ruthenium (III) Porphyrin complex

A note must be taken that the $S_0 - S_1$ notation used in the Jablonski diagrams of organic molecules is now written GS – ^{1}LMCT in this case. It is believed that incident light at about 404 nm promotes one of the electrons in the ligand π bonding orbital to the metal d orbitals, first excited singlet LMCT state. It is also believed that the electron transfer from ^{1}LMCT to ^{3}LMCT, intersystem crossing, is efficient since the intensity of the luminescence is quite high and this could be explained in terms of the heavy atom effect. For heavier atoms like Ruthenium and Rhodium, the spin-orbit interactions become large; as a result the change of spin from the singlet to triplet is favorable.

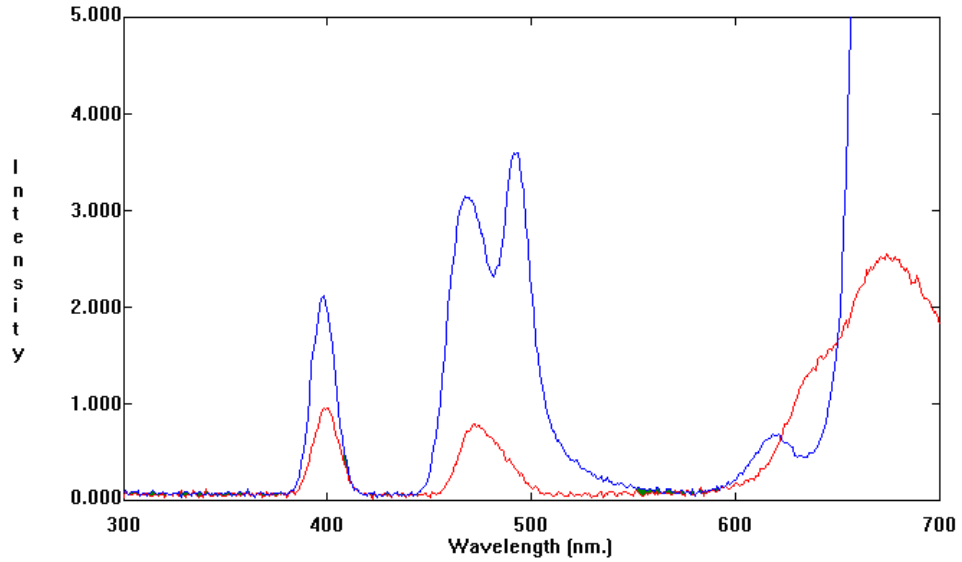

Fig 3.6: Fluorescence spectra of porphyrins in aqueous solution (blue =$TPPS_4$, red = $RuTPPS_4$)

The charge transfer bands were not observed in the electronic absorption spectrum of Rhodium complex therefore the emission is caused by a radiative process from ^{3}LL to GS. This emission band is less intense and more broadened than that of the Ruthenium complex (Figure 3.7). This could be attributed to the fact that Rhodium has smaller radius than Ruthenium.

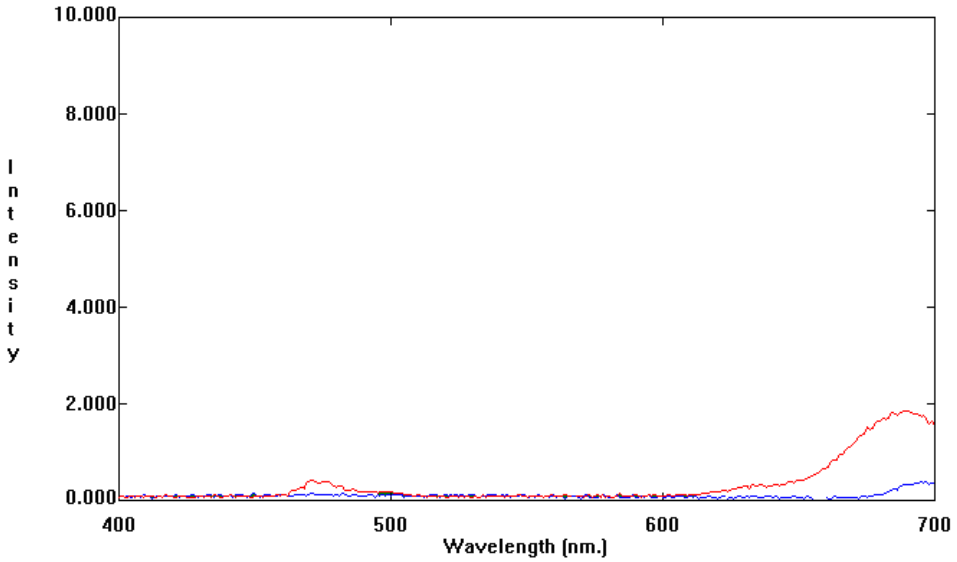

Figure 3.7: Emission spectra of $RuTPPS_4$ (red) and $RhTPPS_4$ (blue)

Table 3.2: Characteristic emission data of ligand $TPPS_4$ and its complexes in aqueous solutions.

Compound	λ1 (nm)-emission	λ2 (nm)-emission
$TPPS_4$	488, 500(split)	620
$Ru(TPPS_4)$	482	685
$Rh(TPPS_4)$	-	690

3.1.3 Infrared Spectroscopy

IR spectrum of TPP recorded as KBr mulls are shown in Figure 3.8. The IR spectrum of TPP showed four major peaks at 3407 cm^{-1}, 1608 cm^{-1}, 1233 cm^{-1} and 818 cm^{-1}. The peak assignment is shown in Table 3.3 below. Nevertheless, the peak assignment is extremely difficult because vibrations of phenyl groups overlap with those of porphyrin core [64]. The aromatic nature of TPP was suggested by the νC-H which appeared above 3000 cm^{-1} i.e. at 3407 cm^{-1} and the appearance of the band at 1608 cm^{-1} which is due to aromatic C=C bond. But the νC-H band clearly overlaps with the broad νN-H stretch band. The band at around 818 cm^{-1} is assigned to the vibrations of the C-H bending modes and the one at 1233 cm^{-1} is due to C-N stretching mode. The other peaks are probably associated with the vibrations of the skeleton of the molecule.

Table 3.3 Characteristic IR peak data for TPP.

Peak Position cm^{-1}	Shape and Intensity	Assignment
3407	broad, low	C-H(aromatic), N-H stretch
1608	broad, low	C=C stretch (aromatic)
1233	broad, low	C-N stretch
818	sharp, low	C-H bend

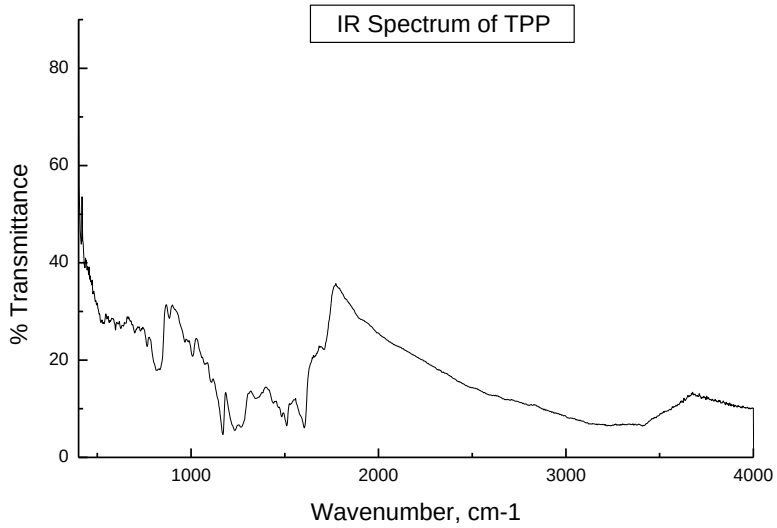

Figure 3.8 IR spectrum of TPP in KBr mull

Introducing the sulphonato groups on the TPP did not result in a remarkable difference in the IR spectrum of TPP as can be observed as per Figure 3.9 i.e. the IR spectrum of TPP did not look quite different from that of $TPPS_4$, except that the peak at around 3400 cm^{-1} is more broadened in $TPPS_4$. This is due to the similar backbone structure in both compounds. Sulphonation of TPP introduced new bonds i.e. C-S, S-O and S=O which their vibrations were not clearly observed. According to literature, the νC-S occurs well below 1000 cm^{-1}(around 587cm^{-1}) thus it may overlap with the rocking vibrations of C-H bond.

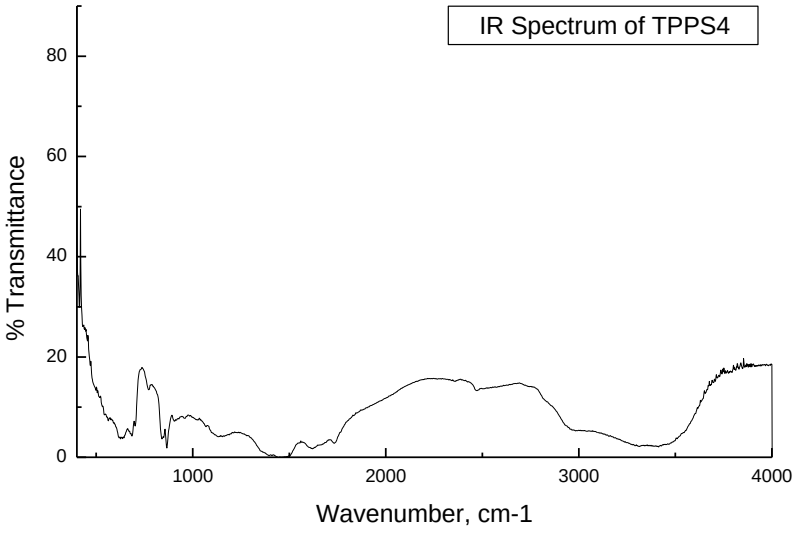

Figure 3.9 IR spectrum of $TPPS_4$ in KBr mull.

The IR spectra of $RuTPPS_4$ and $RuTPPS_4$ in KBr mull are presented in Figure 3.10. A closer look at the IR spectrum shows some resemblances with the IR spectra of both TPP and $TPPS_4$. In general, the bands in the high frequency region (4000-1000 cm-1) are not metal sensitive since they originate in the aromatic ring of the porphyrin. The influence of complexation is distinctly manifested in the spectrum. Noticeable changes in the frequencies of all the vibrations and a redistribution of the intensities of some of them are observed. Most of the bands are characterized by a slight increase in the frequencies which is evidence of a strengthening of corresponding bonds in the molecule and a decrease in their length as per Equation 8, where k is the force constant, c is the speed of light in vacuum and μ is the reduced mass.

$$\nu = \frac{1}{2\pi c}\sqrt{\frac{k}{\mu}} \qquad (8)$$

For instance, in the case of the $TPPS_4$ and $RuTPPS_4$, there is appreciable decrease of about 86 cm^{-1} for the ν_{bend} of the C=C bonds. Some bands retain an unchanged frequency. One should especially take up the band of the nonplanar CH vibrations i.e.

rocking vibrations, situated at 818 cm $^{-1}$ in the selected porphyrins; they correspond to the vibrations of the four CH groups, found in the meso-positions of the molecule.

For $RuTPPS_4$, νN-H stretch and the νN-H bend disappears as there are no longer N-H bonds because the two hydrogens are removed as the metal coordinates.

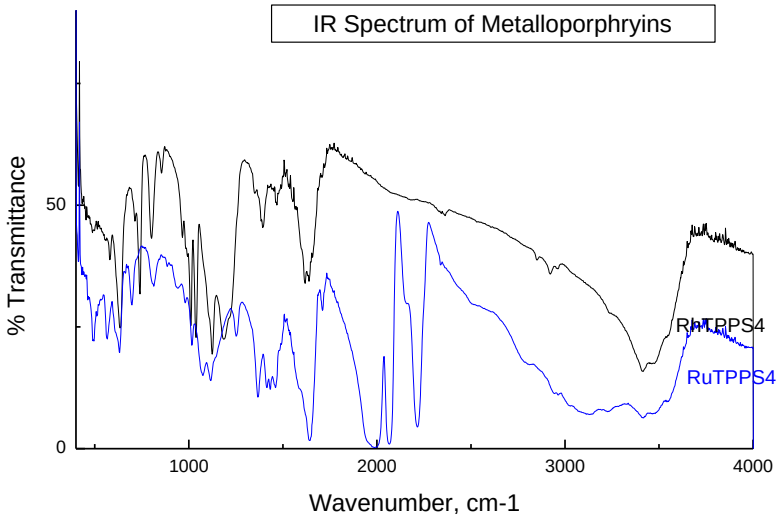

Figure 3.10: IR spectrums of $RuTPPS_4$ and $RhTPPS_4$ in KBr mull

The IR spectrum of $RhTPPS_4$ shown in Figure 3.10 still exhibits some common features with TPP, $TPPS_4$ and $RuTPPS_4$. When compared with the IR spectrum of $RuTPPS_4$, three new intense peaks in the region 2300-1950 cm^{-1} were observed in the spectrum of $RuTPPS_4$. The peaks in this region are usually due to ν(CH_3) and ν(MN-C) where M is the metal centre [8]. But the M-N bond is not observed in the spectrum as it appears in the Raman region. It is therefore believed that the peak at 2185 cm^{-1} is due to ν(CH_3) while the one at 2040 cm^{-1} is due to the ν(N-C) that is bound to the metal. The last peak could be due to C-O. This could be due to the coordination of solvent molecules to the Ruthenium centre. DMF is a weakly coordinating solvent with two potential donor atoms N and O, thus it is a bidentate ligand. It has the following resonance structure:

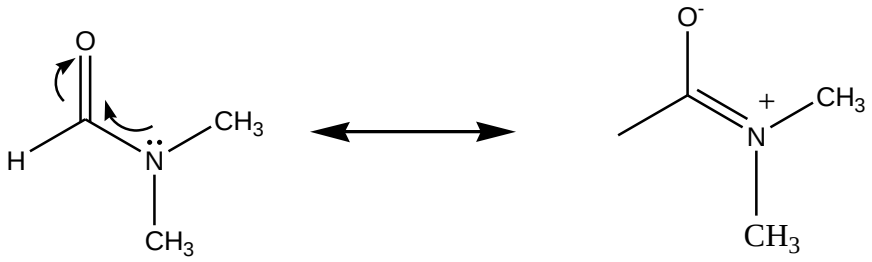

Ruthenium is less electronegative ($\chi_{pauling}$ =2.2) than Rhodium ($\chi_{pauling}$ =2.28), thus the difference in electronegativities of Ru and Rh is rather small to make much difference to the intensity of IR absorption. The d-orbital occupation is more likely to give Ru an extra ligand. It is likely that Ru has coordinated DMF via N in one of the axial positions to give a square- pyramidal geometry. Axial ligation of highly coordinating solvents like DMF, pyridine and dimethyl sulphoxide (DMSO) has been observed before in the phthalocyanine complexes of Ruthenium [60]. Owing to the bulkiness of the ligand, only one axial position is likely to be occupied. Peaks due to axial coordination of solvent were not observed in the $RhTPPS_4$ spectrum. This might be explained by the difference in the bond constants for Ru-N and Rh-N. Ru-N bond constant (480 Nm^{-1}) is larger than Rh-N bond (380 Nm^{-1}), thus the Ru-N bond is stronger [61]. In general, the intensity of the stretching vibrational mode increases as the bond becomes more ionic [62]. Relatively, Ru-N is less ionic than Rh-N thus this may be responsible for the strong appearance of ν(CH3) and ν(MN-C) and their disappearance in the spectrum of $RuTPPS_4$.

3.1.4 Electrochemical Studies of Porphyrins

Cyclic Voltammetry of RuTPPS4 in DMF

Cyclic voltammetry of $RuTPPS_4$ was studied in a carefully purified aprotic medium (DMF) with Tetraethyl ammonium perchlorate (TEAP) employed as an electrolyte and the cyclic voltammogram is shown in Figure 3.11. The compound is electroactive. The CV showed four redox couples; one reduction couple (I, VIII) and three oxidation couples (II, VII), (III, VI) and (IV, V). The observed reduction couple for $RuTPPS_4$ in DMF is located at -373.9 mV vs. Ag/AgCl as per Table 3.4. All these redox couples are believed to correspond to ring reduction and oxidation for $TPPS_4$ since the metal centre Ru^{3+} is redox inactive [63]. The electrochemistry of metalloporphyrins is known to depend

on a variety of factors, some of which are related to the nature of the macrocycle, some to the central metal ion and some to the solution conditions. The number of observed redox couples i.e four is in agreement with the number of peaks observed in the cyclic voltammogram of a metal inactive centered porphyrin [64].

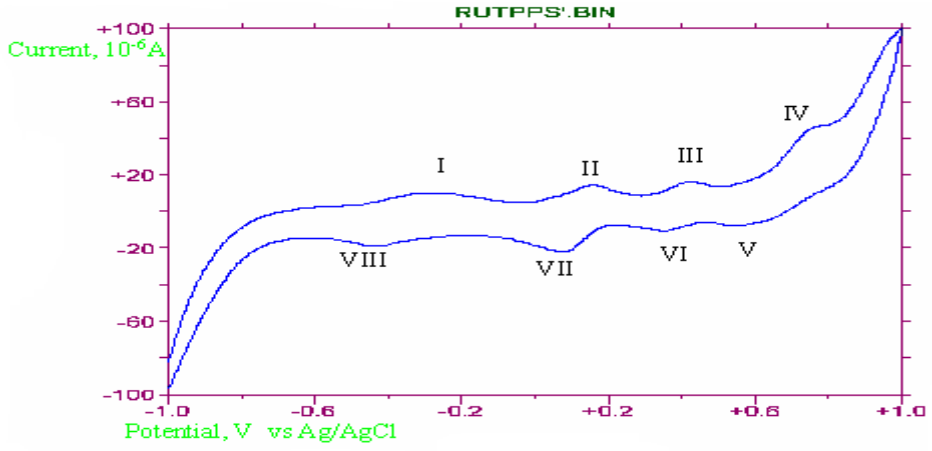

Figure 3.11: The Cyclic voltammogram of $RuTPPS_4$ in DMF on a platinum electrode; scan rate 100mV/s, sensitivity 10μA/V. Supporting electrolyte was TEAP. Scan direction was from –ve to +ve potential.

The CV of $RuTPPS_4$ run on the platinum electrode show the rising portion of the first two waves (II and III) on the positive potentials which have a shape characteristic of a reversible one-electron process, and these peaks appear to be reversible. The peak separation between the respective cathodic (I) and anodic peak (VIII) gives the number of electrons as 1 for this first couple, which is in good agreement with the shape of this peak. The electron transfer process could be written as;

$$RuTPPS \rightarrow RuTPPS^{\cdot +} + e^{-} \qquad (9)$$

It is often instructive to consider peak ratio. For a reversible electrochemical process, this ratio approaches unity (1).The ratio of cathodic to anodic current for this first peak is nearly 2, i.e.

$$\frac{I_{pc}}{I_{pa}} = \frac{2.297 \text{ X } 10^{-5}}{1.044 \text{ X } 10^{-5}}$$

$$= 2$$

This also suggests a quasi-reversible process. This value differs significantly from 1 and this is typical of an electrochemical process coupled with a chemical process. The first of the two is reversible and results in the formation of the porphyrin dianion. All the waves appear to be reversible or quasi-reversible steps. The electrochemical data of the complex is summarized in Table 3.4.

Table 3.4 Voltammetric data for $RuTPPS_4$ in DMF at 26°C.

Peak	E° mV	Peak separation ΔE (mV)	Number of electrons	Peak Current Ratio
I	-373.9	157.1	-	-
II	+167.0	73.1	0.801	1.388
III	+384.7	70.5	0.837	0.623
IV	+736.6	33.3	1.771	0.065

Cyclic Voltammetry of $RuTPPS_4$ in aqueous medium

The CV of $TPPS_4$ in aqueous medium is presented in Figure 3.12. $TPPS_4$ shows electrochemical activity in aqueous medium. Two segments were observed for $TPPS_4$. The first voltammetric wave which appeared at E_{pc} = -739mV seems to be irreversible. The irreversibility of the process is indicated by the absence of an anodic peak associated with this step and this suggests that a rapid, irreversible chemical reaction has followed the reductive electron transfer .The second wave located at E_p = +656 mV seems to be irreversible as the reverse peak is observed at Ep = -250 mV. The peak separation therefore is vey big.

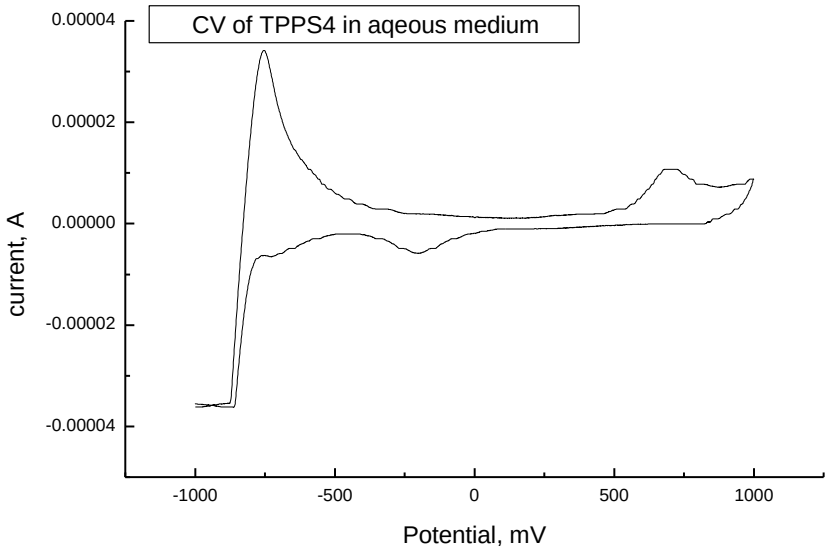

Figure 3.12 Cyclic voltammogram of $TPPS_4$ in aqueous medium run at the scan rate of 50mV/s, sensitivity of 10 μA/V on a platinum electrode. Scan direction was from –ve to +ve potential.

The CV of $RuTPPS_4$ in aqueous medium is shown in Figure 3.13. In the CV of $RuTPPS_4$, an anodic peak on the negative potentials (E_p = -489 mV) and a cathodic peak in the positive potentials (E_p = +787mV) are observed. These are believed to be reduction and oxidation couples of the porphyrin ring as the metal centre is redox inactive under the experimental conditions. This can be confirmed by spectroelectrochemistry. The oxidation redox couple is also observed in the $TPPS_4$, but with a positive shift of the cathodic wave and a negative shift of the anodic wave. The quasireversibility of this process is suggested by the peak separation of 61 mV. The current-voltage curves obtained in this way appear deceptively simple because several of the chemical steps associated with electron transfer in the porphyrins are slow with respect to the time scale of the experiment [65].

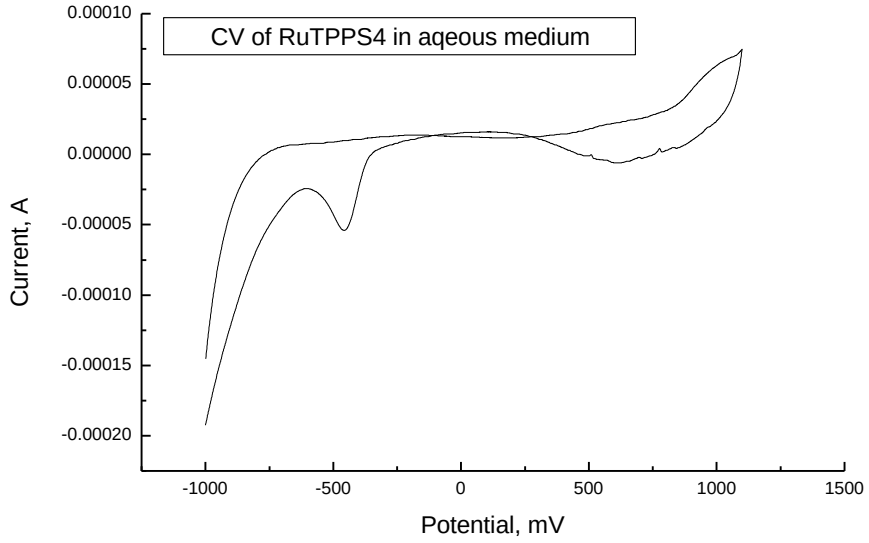

Figure 3.13: Cyclic voltammogram of RuTPPS4 in aqueous medium run at the scan rate of 50mV/s, sensitivity of 10 μA/V on a platinum electrode. Scan direction was from –ve to +ve potential.

3.1.5 Magnetic Properties of the Complexes

Since the metal centres i.e Ru^{3+} and Rh^{3+} in the complexes have f orbitals, the equation which takes into account orbital contribution to the overall magnetic moment (μ_{eff}) was used.

$$\mu_{eff} = \left(n\,(n+2) + L\,(L+1)\right)^{1/2} \qquad (10)$$

Where n is the number of unpaired electrons and L is the sum of magnetic quantum number (l) rather than the spin only magnetic moment $\mu_{s.o}$.

$$\mu_{s.o} = \left(n\,(n+2)\right)^{1/2} \qquad (11)$$

The observed μ_{eff} for $RuTPPS_4$ is 6.718 BM and is close to the calculated value of 6.708 BM which ultimately gives the number of unpaired electrons as 1.034 which is rounded to 1.Thus $RuTPPS_4$ is a low spin, paramagnetic complex and the electron configuration of Ru^{3+} in an octahedral field is $t_{2g}^5e_g^0$ i.e

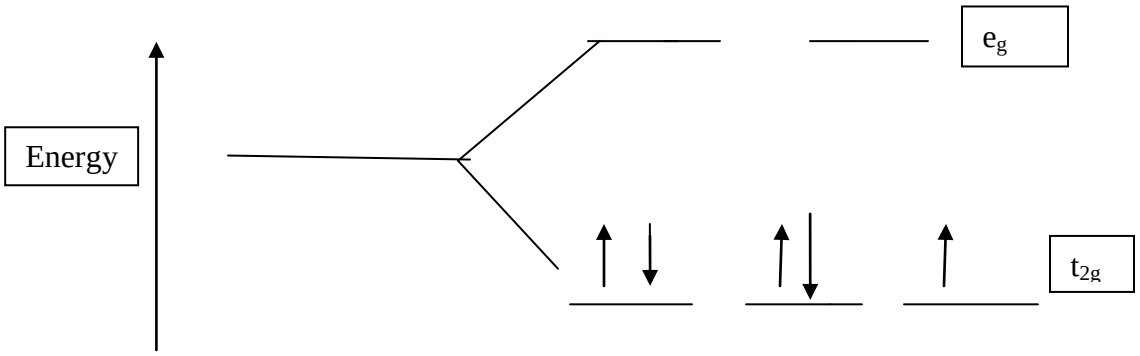

Fig 3.14: Spin state of a low spin d^5 system in an octahedral field.

Likewise, the calculated μ_{eff} for $RhTPPS_4$ is 6.484 BM (Table 3.5) is close to the expected one 6.481 BM (Table 3.5). As a result, the number of unpaired electrons is 0.021 which is approximated to 0. Thus $RhTPPS_4$ is a low spin, diamagnetic complex and the electron configuration of Rh^{3+} in an octahedral field is $t_{2g}^6e_g^0$. It is observed that both $RuTPPS_4$ and $RhTPPS_4$ complexes are of low spin, and this is likely to be attributed to the nature of the ligand, $TPPS_4$ which is likely to be a π-acceptor ligand. For a complex with π-acceptor ligands, increased π-acceptance stabilizes the t_{2g} orbitals, increasing the crystal filed splitting energy as confirmed by absorption spectroscopy and such a complex is likely to be low spin.

Table 3.5 Magnetic Data for the complexes at 20 °C

Complex	χ_m corrected	μ_{eff} calculated	μ_{eff} observed	n
$RuTPPS_4$	1.922×10^{-2}	6.718	6.708	1.034
$RhTPPS_4$	1.791×10^{-2}	6.484	6.481	0.021

3.2 Characterization of Polyaniline

3.2.1 Catalytic Synthesis of Polyaniline

The reaction of aniline and hydrogen peroxide in acidic medium (pH = 2) carried out in the presence of $RuTPPS_4$ following the method outlined in section 2.4 produced a blue solution after 72 hours and after dialysis and drying under the fume hood (as the thermal stability of the polymer was not known); 2.0 g of PANi was obtained. The blue colour of the solid indicated that we have actually prepared the Emeraldine form of PANi [66]. Protonation with hydrochloric acid resulted in bluish green solution. It was observed that after 72 hours, the uncatalysed reaction have not yet produced desirable results as per Figure 3.15. This shows that the reaction was slowly occurring in a conical flask containing no $RuTPPS_4$ and much slower in a flask containing no $RuTPPS_4$ and SPS which served as the template. Thus this evidences the catalytic properties of $RuTPPS_4$.

Figure 3.15 Catalysis experiment after 72 hours.

The reaction carried out in the presence of $RhTPPS_4$ resulted in greenish-blue solution after a much longer period (96 hours) and 0.36 g of the polymer was obtained. This

suggested that $RuTPPS_4$ was a better catalyst for the polymerization of aniline than its Rhodium counterpart. The catalytic turnover (TON) which is the number of moles of product per mole of catalyst was not calculated as the chain length of the polymer was not known but qualitatively, it was clear that this number was quite high for $RuTPPS_4$. This indicated that there are more catalytic cycles when $RuTPPS_4$ served as the catalyst. Similarly catalytic turnover frequency (TOF) which is the catalytic turnover per unit time was clearly high for $RuTPPS_4$ as the reaction produced desirable results within a shorter period (72 hours).

$RuTPPS_4$ seemed a better catalyst for polymerization of aniline possibly because of relative ease of oxidation of Ru^{3+}. It is assumed that the polymerization of aniline in the presence of $RuTPPS_4$ and $RhTPPS_4$ follows the same radical pathway, as the one proposed by Nabid *et al.* [23], except here the rate determining step is assumed to be the oxidation of the metal centre by hydrogen peroxide to form an oxo radical. The proposed mechanism for catalyzed polymerization of aniline is shown in Scheme 5.

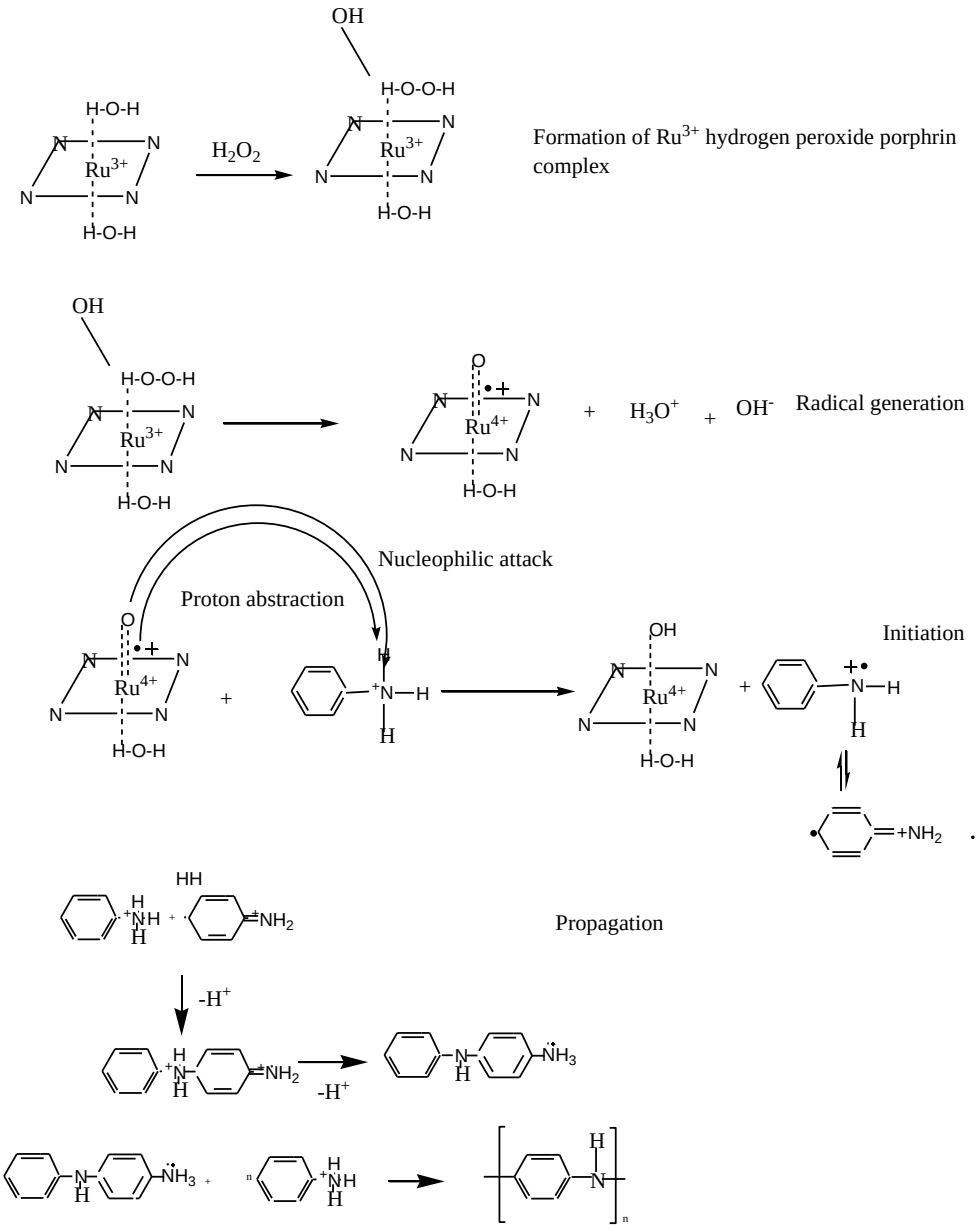

Scheme 5: Proposed Mechanism for polymerization of aniline in the presence of $RuTPPS_4$.

3.2.2 IR Spectrum of PANi

IR Spectrum of Aniline

The structural characteristics of aniline were investigated by FTIR spectroscopy in the region 4000-400 cm^{-1} in KBr mull. The peak located at 3354 cm^{-1} is assigned as C-H aromatic (Figure 3.16).

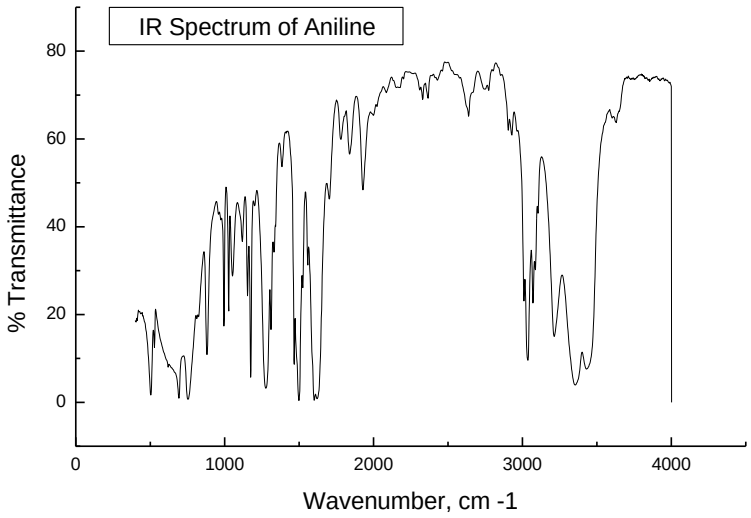

Figure 3.16: FTIR spectrum of aniline in KBr mull.

IR Spectrum of Polyaniline

The structural characteristics of PANi were also investigated by FTIR spectroscopy from 4000-400 cm^{-1} in KBr Mull and the spectrum is shown in Figure 3.17. The bands at ca 1600 cm^{-1} are indicative of the stretching vibrations in the quinoid rings [23].

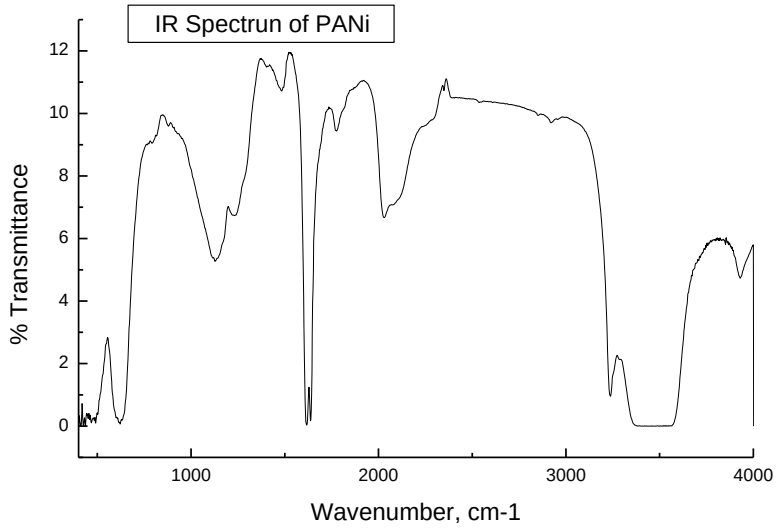

Figure 3.17: FTIR spectrum of Polyaniline.

The spectrum of aniline and its polymer showed similar features because they have the same basic unit .The major difference between the spectrum of aniline and polyaniline is in the 3400-3000 cm^{-1} region. In this region, there is a broad band and this suggests the presence of –NH groups within the aniline and PANi. The band broadened upon polymerization and its position shifted to lower frequency.

3.2.3 Absorption spectroscopy of the PANi

Figure 3.18 shows the absorption spectrum of PANi in water. It showed three (3) clear bands at 439, 547 and 640 nm respectively. The band at 439 nm corresponds to the reduced state (leucoemeraldine) of PANi (π- π* transition) [67]. The second band at 547 nm corresponds to a partially oxidized form of PANi while the third one at 640 nm is due to the fully oxidized pernigraniline form and is characterized by a broad band.

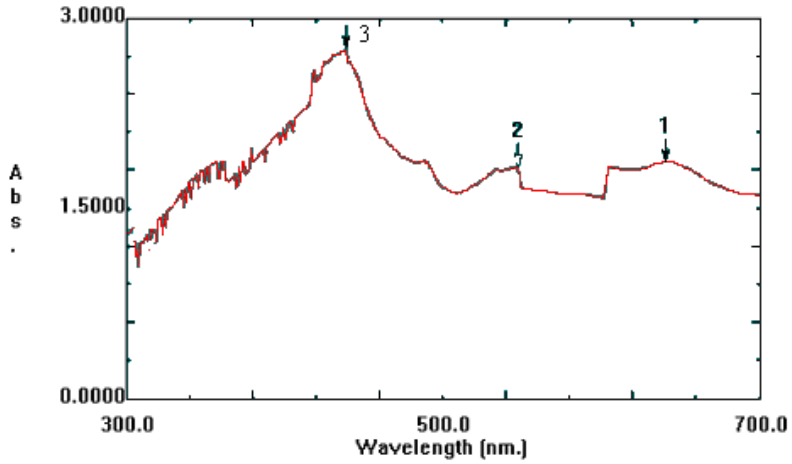

Figure 3.18: Electronic Absorption spectrum of PANi

3.2.4 Cyclic Voltammetry of PANi

Cyclic Voltammetry of PANi was studied in 1M HCl. Best results were obtained at 1µA/V sensitivity and at a scan rate of 5 mV/s. A typical cyclic voltammogram is shown in Figure 3.19. A careful inspection of the CV shows that there are two anodic and one cathodic peak. Emphasis was placed on the first redox couple A/A$^{/}$. This couple with the oxidation peak (A) at + 109 mV relates to the transition from the fully reduced leucoemeraldine to the half oxidized emeraldine which is the most conductive redox transition in polyanilines [68].

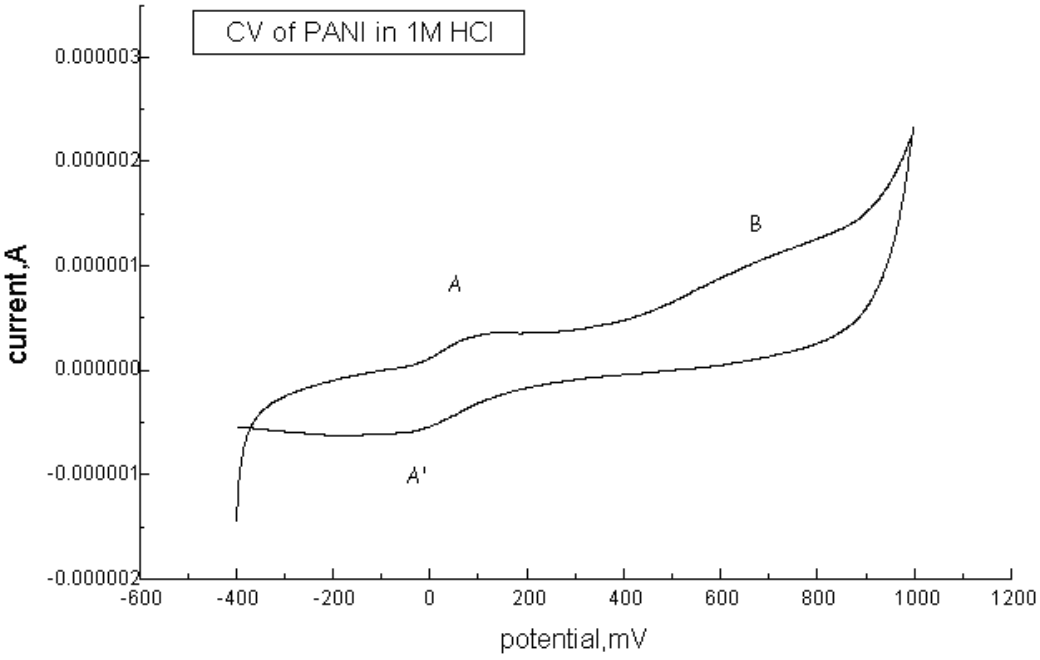

Figure 3.19: CV of PANi in 1M HCl at a platinum electrode. Scan direction was from –ve to +ve potential.

The number of electrons transferred was estimated using the peak separation of 67 mV and it was found to be one electron transfer system while the ratio of anodic peak current (I_{pa}) to cathodic peak current (I_{pc}) was 1.20 which is not exactly unity as required for a fully reversible one electron transfer, and therefore a quasireversible electron transfer mechanism is suggested. The results are summarized in Table 3.6

Table 3.6 Electrochemical Data for PANi in 1 M HCl

Peak	E_p mV	Peak separation ΔE (mV)	Number of electrons	Peak Current Ratio
A	+109.9	67.1	1.14	1.20
A/	-42.1	67.1	1.14	1.20
B	+712.0	-	-	-

The peak potentials and the corresponding currents in the CV's vary as the scan rates vary as per Figure 3.20, indicating that the polymer is electroactive and that the charge transportation was taking place along the polymer chain. The system displayed a progressive shift in anodic peak potential towards more positive values coupled with shift in cathodic peak potentials to less positive (i.e. more negative) values with increase in the scan rate. The peak separations increased slightly at 5mV/s to at 50mV/s coupled with increase in the magnitude of the peak currents, but with a large increase in the cathodic currents. Using the Randles-Sevcik equation;

$$i_p = (2.686 \times 10^5)\, n^{3/2} A c D^{½} \nu^{½} \qquad (12)$$

The linear dependence of the peak currents on the scan rate is observed which indicated this electron transfer is diffusion controlled (Figure 3.21). The diffusion coefficient D was not evaluated from the slope as the concentration of PANi solution was not known. This is because the molar mass of the polymer was unknown.

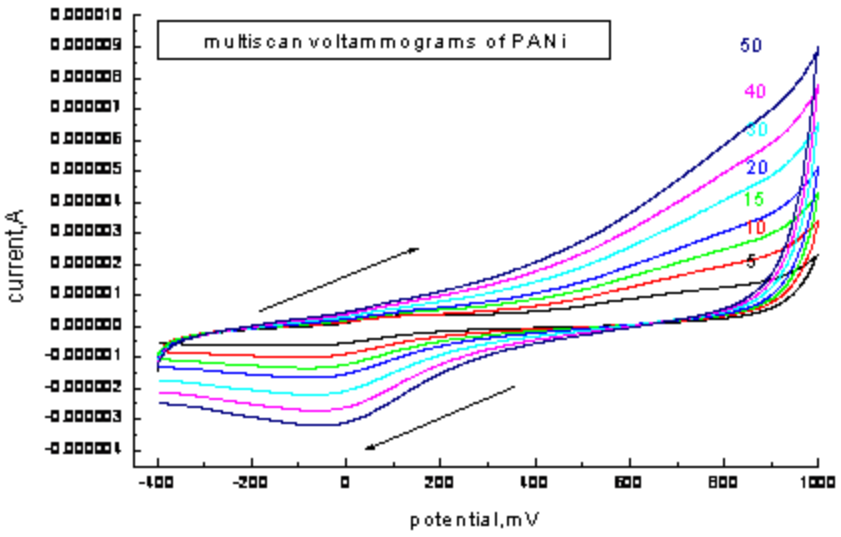

Figure 3.20 Multiscan voltammogram of PANi in IM HCl solution at 5, 10, 15,20,30,40 and 50mV/s.

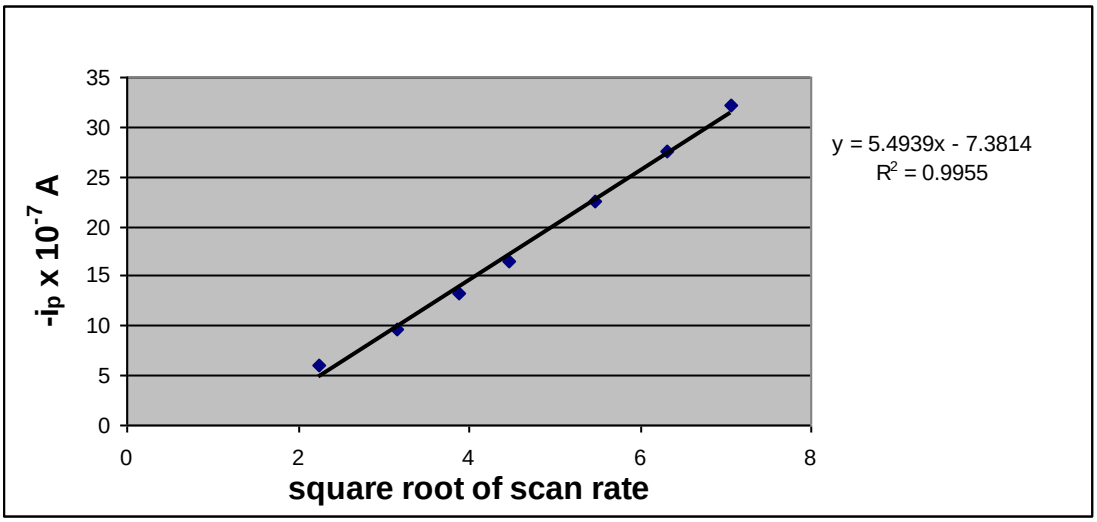

Figure 3.21: A plot of cathodic peak currents (I_{pc}) versus square root of scan rate.

3.1.5 Morphology of the polymer

The morphology of PANi was investigated by both SEM and TEM characterization. A closer look at the SEM images revealed that we have synthesized the clews .There are a large number of honeycombed clews whose diameter is about 5 micrometer; furthermore, these clews are composed of interconnected network fibril with characteristic cross-sectional fibril dimensions of a few tens of nanometers. Moreover, PANi nanostructures look like cauliflower bunches.

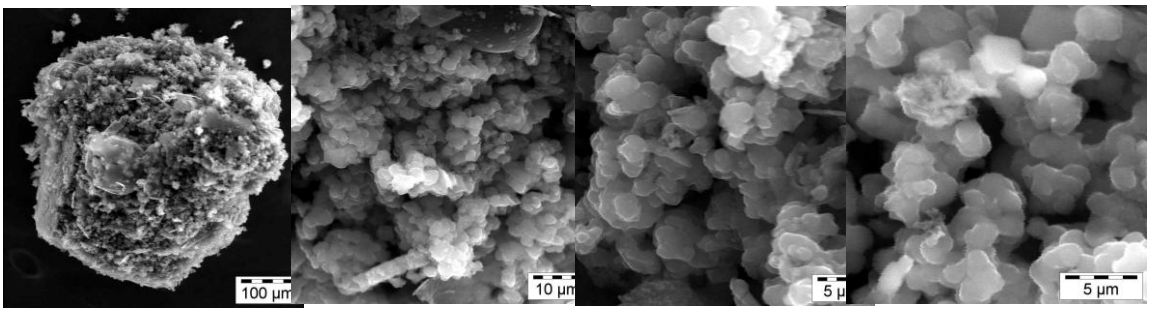

X 220 X 2000 X 3000 X 6000

Fig3.22: SEM images of high molecular weight PANI at both low and high magnifications.

The TEM results confirmed that the nanostructure cauliflower PANi is porous. This is indicated by the light spots in the TEM image. The black shaded part could be due to the sulphonated polystyrene which served as the template.

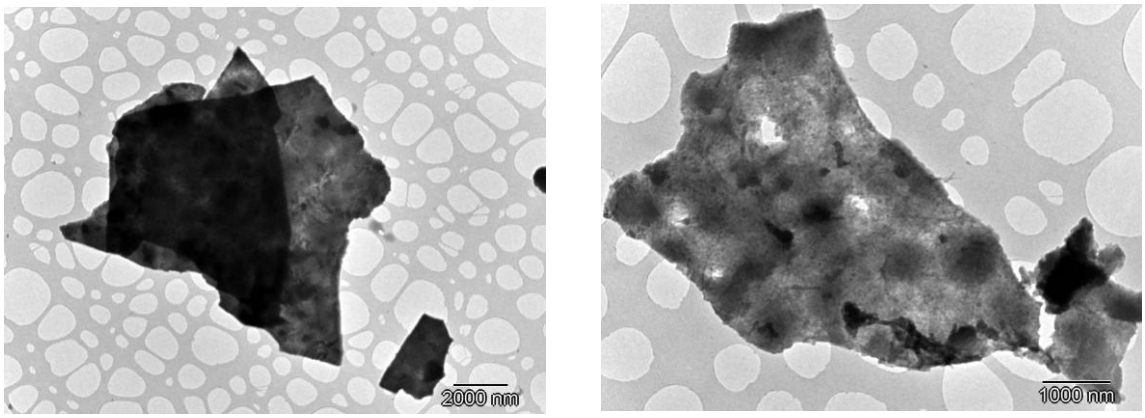

X 8k X 20K

Figure 3.23: TEM images of PANi at both low and high magnifications.

CHAPTER 4

CONCLUSIONS AND FUTURE AVENUES

The selected catalysts for polymerization of aniline, $RuTPPS_4$ and $RhTPP_4$ were synthesized with satisfactory yields (~ 60%) and characterized. The low percentage yields were attributed to side reactions. For instance, the likely condensation reaction between the pyrrole and the propionic acid could have reduced the yield. Facile synthesis of water soluble PANi utilizing water soluble $RuTPPS_4$ and $RhTPPS_4$ as the catalysts was successfully carried out under ambient conditions. $RuTPPS_4$ seemed a better catalyst due to high TON and TOF. In summary, a facile chemical method to synthesize the uniform and ordered nanoparticles of PANi was introduced. In this particular synthetic condition, a novel morphology has been noticed: numerous of honeycombed clews are found, which consist of interpenetrating fibrils whose diameters are no more than one hundred nanometers. The morphology of PANi clews synthesized in the presence of water soluble metalloporphyrins of Rhodium and Ruthenium show the reaction mechanism has an orientation effect. The CV results indicate that the polymer is electroactive and electrochemical interrogation of the polymer by cyclic voltammetry showed that it exhibits a quasi-reversible electrochemistry. The PANi microspheres with nanostructured surfaces may provide potential applications as chemical/electrochemical sensors, actuators and nano/micro photoelectronic devices. The re-usability of these $M(III)TPPS_4$ systems was not studied due to financial and time constraints.

Future work therefore, will target the detection and quantification of analytes of interest like sulphur containing compounds using these honeycombed PANi nanostructures. Sulphur compounds are believed to be one of the major pollutants of the environment produced primarily in the dumpsites. When one passes near Thetsane and Tsosane landfill sites in Maseru, the pollution is evidenced by the pungent smell. Sulphite is widely employed as an antioxidant and inhibitor of bacterial growth in the food and beverage industry, in pharmaceutical formulations and in paper pulp production. The sulphite is also associated with sulphur dioxide pollutant in air. Methods for the rapid and precise determination of sulphite have been developed in recent years; most of them

using indirect detection methods, such as enzymatic, bromimetric or iodimetric methods. The direct detection of sulphite using conventional electrodes is not a simple task. The oxidation of sulphite is thermodynamically feasible, but the reaction kinetics are too slow, and consequently the overpotentials are normally very high. Thus the use of water soluble PANi as mediator i.e. electrocatalyst, may reduce these high overpotentials and/ or improve the electrochemical response.

REFERENCES

1. Suslick, KS, Van Duesen-Jeffries, S, *"Shape Selective Oxidation Catalysis" Comprehensive Supramolecular Chemistry*, **1996**, 5th ed, Elsevier Publishers, Oxford; 141-170

2. Falk, JE, *Porphyrins and Metalloporhyrins*, **1975,** Elsevier, New York

3. Beletskaya, I, Tyurin, SV, Tsivadze, A, Guilard, R, Stern, C, *Chemical Reviews,* **2009,** *109;* 1659–1713

4. Biesaga, M, Pyrzyn'ska, K, Trojanowicz, M, *Talanta*, **2000**, 51; 209-224

5. Berezin, BD, Enikolopjan, NS, *Metalloporphyrins;* Nauka: Moscow, **1988**

6. Shkirman, SF, Solovev, N, Kachura, TF, *Journal of Applied Spectroscopy*, **1999**, 66, 1; 68-75

7. Smith, KM, J*ournal of Photochemistry and Photobiology B*, **2001**. 64; 144

8. Nakamoto, K, *Infrared and Raman Spectra of Inorganic and Coordination Compounds Part I: Theory and Applications in Inorganic Chemistry*. Wiley, **1997**; 214-215

9. Chang, D, Malinski, T, Ulman, A, Kadish, KM, *Inorganic Chemistry*, **1984**, 23; 817-824

10. Becker, JY, Dolphin, D, Paine, JB, Wijeskera, T, *Journal of Electroanalytical Chemistry*, **1984**, 164; 335-346.

11. Yamazaki, S, Senoh, H, Yasuda, K, *Electrochemistry Communications,* **2009**, 11, 6; 1109-1112

12. Gervaldo, M, Funes, M, Durantin, J, Fernandez, L, Fungo, F, Otero, L, *Electrochimica Acta*, **2010**, 55, 6; 1948-1957

13. Li, Y, Rizzo, A, Salerno, M, Mazzeo, M, Huo, C, Wang, Y, Li, K, Cingolani, R, Gigli, G, *Applied Physics Letter,* **2006**; 89, doi:10.1063/1.2335511

14. Finikova.O, Chen.P, Ou.Z., Kadish.K, Vinogradov.S, *Journal of Photochemistry and Photobiology A,* **2008**, 198, 1; 75–84.

15. Wang, X, Chen, H, Zhao, Y, Chen, X, Wang, X, Chen, X, *Trends in Analytical Chemistry,* **2010,** 29, 4; 319-338

16. Pushpan, SK, Venkatraman, S, Anand, VG, Sankar, J, Parmeswaran, D, Ganesan, S, Chandrashekar, TK, *Current Medicinal Chemistry - Anti-Cancer Agents,* **2002**, 2, 2; 187-207

17. Buchler, JW, Dreher, C , Künzel, FM, *Metal Complexes with Tetrapyrrole Ligand III*, **1995**, 2; 84

18. Cocchi, M, Virgili, D, Fattori, V, Rochester, DL, Williams, JAG, *Advanced Chemical Materials*, **2007**, 17, 2; 285 – 289

19. Kadish, KM, Smith .K, Guilard.R, *'Medical Aspects of Porphyrins', The Porphyrin Handbook*, **1999**, 14, Academic Press; 2-4

20. Sheldon, RA. *Metalloporphyrins in Catalytic Oxidations*, New York: Marcel Dekker Inc. **1994**; 340-341

21. Abe, T, Kaeko, M, *Progress in Polymer Science*, **2003**, 28; 1441

22. Buchler, JW, Dreher.C , Künzel.FM, *Metal Complexes with Tetrapyrrole Ligand III*, **1995**, 2; 84

23. Nabid, MR, Zamiraei, R, Sedghi, R, Safari, N, *Reactive &Functional polymers*, **2009**, 69, 5;319-324

24. Letheby, H, *Journal of Chemical Society*, **1996**, 15; 5017-5047

25. Heeger, JA, *Reviews of Modern Physics*, **2001**, 73; 681-700

26. Morton-Blake, DA, Corish, J, *Electroactive Polymer Electrochemistrty Part II Methods and Applications Plenum*, New York, **1996**

27. http://wokinfo.com/products_tools/multidisciplinary/webofscience/ date accessed 07/04/2011

28. Huang, J, Virji, S, Weiller, BH, Kaner, R, *Journal of American Chemical Society*, **2003**, 125; 314-315

29. Palaniappan, S, John, A, *Progress in Polymer Science*, **2008**, 33; 732-758

30. Skotheim, TA, Elsenbaumer, RL, Reynolds, JR, *Handbook of Conducting Polymers*, **1998,** Dekker, New York; 823–1073

31. Konyushenko, EN, Stejskal, J, Šednková, I, Trchová, M, Sapurina, I, Cieslar, M, Prokeš, J, *Polymer International*, **2006**, 55; 31

32. Bejan, D, Duca, A, *Croatia Chemica Acta*, **1998**, 71; 745

33. MacDiarmid, AG, Jones, EW, Norris, ID, Gao. J, Johnson, AT, Pinto, NJ, *Synthetic Materials*, **2001**, 119; 27

34. Osterholm, JE, Cao, Y, Klavetter, F, Smith, P, *Polymer*, **1994**, 35; 2902-2906

35. Kinlen, PJ, Liu, J, Ding, Y, Graham, CR, Remsen, EE, *Macromolecules*, **1998**, 31; 1735-1744

36. Paul, RK, Pillai, CKS, *Polymer International*, **2001**, 50; 381-386

37. Swapna, RP, Sathyanarayana, DN, Palaniappan, S, *Macromolecules*.**2002**, 53; 4988-4996

38. Shreepathi, S, Holze, R, *Chemical Materials*, **2005**, 17; 4078-4085

39. Bicak, N, Karagoz, B, *Journal of Polymer Science Part A: Polymer Chemistry*, **2006**, 44; 6025-6031

40. Michira.I, Klink.M, Akinyeye.O, Somerset.V, Sekota.M, Al-Ahmed.A, Baker.P, Iwouha.E, *Recent Advances in Analytical Chemistry*, **2007**; 137-165 ISBN:978-81-7895-274-1

41. Nabid, MR, Sedghi, R, Jamaat, PR, Safari, N, Entezami, A, *Journal of Applied Polymer Science*, **2006**, 102; 2929–2934

42. Singh, V, Mohan, S, Singh, G, Pandey, PC, Prakash, R, *Sensors and Actuators B*, **2008**, 164; 99-106

43. Yang, CH, Huang, LR, Chih, YK, Lin, WC, Liu, FJ, Wang, TL, *Polymer*, **2007**, 48; 3237-3247

44. Guo, Q, Yi, C, Zhu, L, Yang, Q, Xie Y, *Polymer*, **2005**, 46; 3185-3189

45. Kobayashi, S, Uyama, H, kimura, S, *Chemical Review*, **2001**, 101; 3793-3795

46. Mejias, L, Reihmann, MH, Sepulveda-Boza, S, Ritter, H, *Macromolecules Bioscience*,. **2002**, 2; 24-32

47. Xue, W, Fang, K, Qiu, H, Mao, W, *Journal of Synthetic Materials*, **2002**, 130; 155

48. Belogorokhov, AI, Bozhko, SI, Ionov, AM, Chaika, AN, Trofimov, SA, Rumyantsev, VD, Vyalikh, D, *Journal of Surface Investigation. X-ray, Synchrotron and Neutron Techniques*, **2009**, 3, 6; 912–916

49. Busby, CA, Dinello, KR, Dolphin, D, *Canadia Journal of Chemistry*. **1975**, 53; 1554-1555

50. Adler, AD, Longo, FR, Finarelli, JD, Goldmacher, J, Assour, J, Korsakoff, L, *Journal of Organic Chemistry*, **1967**, 32, 2; 476–476

51. Kubat.P,Mosinger.J, *Journal of Photochemistry and Photobiology A,*. **1996**, 96; 93-97

52. Rumlevora-Lipsova, A, Barek, J, Drasa, P, Zelenka, K, Peckova, K, *International Journal of Electrochemical Science*, **2003**, 2; 235-237

53. Tanaka, M, *Pure Applied Chemistry*, **1983**, 55; 15

54. Gadonas, R, Vaicaitis, V, Frolov, DA, Rotomskis, R**,** *Chemical Physics Letter*, **1986,** 9; 603-606

55. Pasternack, F, Collings, PJ, *Science*, **1995**, 5, 269; 935-939

56. Pasternack, F, Hubber, PR, Boyd, P, Engaser, G, Francesconi, L, Gibbs, E, Fasella, P, Venturo, GC, Hinds, L, *Journal of American Chemical Society*, **1972,** 5, 94**, ;**4511-4517

57. Kalyanasundaram, K, Neumann-Spallart, M**,** *Journal of Physical Chemistry*, **1982,** 86; 5163-5169

58. Liu, J, Huang, J, Fu, B, Zhao, P, Yu, H, Ji, L, *Spectrochimica.Acta A: Molecular and Biomolecular Spectroscopy*, **2007**, 67, 2; 391-394

59. Nakamoto.K, *Infrared and Raman Spectra of Inorganic and Coordination Compounds Part I: Theory and Applications in Inorganic Chemistry*, Wiley, **1997**; 214-215

60. Dolphin, D, James, BR, Murray, AJ, Thornback, JR, *Canadian Journal of Chemistry*, **1980**, 58; 1125-1132

61. Terrasse, JM, Poulet, H, Mathieu, JP, *Spectrochimica Acta*, **1964**, 20; 305

62. Nakagawa, I, Shimanouchi, T, *Spectrochimica Acta*, **1966**, 22; 759

63. Fisher, JM, Potter, RJ, Barnard, CFJ, *Platinum Metals Reviews*, **2004**, 48, 3; 101

64. Kadish, KM, Van Caemelbecke, E, *Journal of Solid State Electrochemistry*, **2003**, 7; 254-258

65. Kadish, KM, Van Caemelbecke, E, *Electrochemistry of Metalloporphyrins in Encyclopedia of Electrochemistry*, **2007**, Wiley

66. Feast, WJ, *Polymer*, **1996,** 37, 22; 5017–5047

67. Widera, J, Palys, B, Bucowska, J, Jackowska, K, *Synthetic Materials*, **1998**, 94; 265

68. Klink, M, Akinyenye, R, Somerset, V, Sekota, M, Baker, P, Iwuoha, E, *Material Science Forum*, **2010**, 657; 231-248